DSF-2012-6 (Napoli), MZ-TH/12-50 (Mainz)

February 6, 2022

Rare baryon decays $\Lambda_b \to \Lambda\ell^+\ell^-$ $(\ell = e, \mu, \tau)$ and $\Lambda_b \to \Lambda\gamma$: Differential and total rates, lepton– and hadron–side forward–backward asymmetries

Thomas Gutsche,[1] Mikhail A. Ivanov,[2] Jürgen G. Körner,[3] Valery E. Lyubovitskij *,[1] and Pietro Santorelli[4,5]

[1] *Institut für Theoretische Physik, Universität Tübingen, Kepler Center for Astro and Particle Physics, Auf der Morgenstelle 14, D-72076, Tübingen, Germany*

[2] *Bogoliubov Laboratory of Theoretical Physics, Joint Institute for Nuclear Research, 141980 Dubna, Russia*

[3] *PRISMA Cluster of Excellence, Institut für Physik, Johannes Gutenberg-Universität, D-55099 Mainz, Germany*

[4] *Dipartimento di Fisica, Università di Napoli Federico II, Complesso Universitario di Monte Sant'Angelo, Via Cintia, Edificio 6, 80126 Napoli, Italy*

[5] *Istituto Nazionale di Fisica Nucleare, Sezione di Napoli, 80126 Napoli, Italy*

Using the covariant constituent quark model previously developed by us we calculate the differential rate and the forward–backward asymmetries on the lepton and hadron side for the rare baryon decays $\Lambda_b \to \Lambda\ell^+\ell^-$ $(\ell = e, \mu, \tau)$ and $\Lambda_b \to \Lambda\gamma$. We use helicity methods to write down a three–fold joint angular decay distribution for the cascade decay $\Lambda_b \to \Lambda(\to p\pi^-) + J_{\rm eff}(\to \ell^+\ell^-)$. Through appropriate angular integrations we obtain expressions for the rates, the lepton–side forward–backward (FB) asymmetry and the polarization of the daughter baryon Λ leading to a hadron–side forward–backward asymmetry. We present numerical results on these observables using the covariant quark model and compare our results to the results of other calculations that have appeared in the literature.

PACS numbers: 12.39.Ki,13.20.He,14.20.Jn,14.20.Mr

Keywords: relativistic quark model, light and bottom baryons, rare decays, angular distributions, asymmetries

I. INTRODUCTION

In a recent paper the CDF Collaboration has reported on 24 events of the rare baryon decay $\Lambda_b \to \Lambda + \mu^+\mu^-$ [1]. The collaboration measures the total branching ratio and gives first results on the q^2–spectrum. This experimental result is quite remarkable since, given the measured branching ratio of 1.73×10^{-6}, the CDF collaboration must have had a data sample of at least 42 million Λ_b's. The physics of heavy baryon decays appears to have entered a new era with this experimental result. With the LHC running so well, many more Λ_b's will be recorded by e.g. LHCb in the near future which makes the study of rare Λ_b decays a worthwhile enterprise. The decay $\Lambda_b \to \Lambda\,\ell^+\ell^-$ can be considered to be a welcome complement to the well–analyzed rare meson decays $B \to K^{(*)}\,\ell^+\ell^-$, $B_s \to \phi\,\ell^+\ell^-$ etc. to study the short– and long–distance dynamics of rare decays induced by the transition $b \to s\,\ell^+\ell^-$.

There have been a number of theoretical papers on the rare $\Lambda_b \to \Lambda$ baryon decays involving the one-photon mode $\Lambda_b \to \Lambda\gamma$ and the dilepton modes $\Lambda_b \to \Lambda\,\ell^+\ell^-$ $(\ell = e, \mu, \tau)$. They use the same set of (penguin) operators or their non–Standard Model extensions to describe the short distance dynamics but differ in their use of theoretical models to calculate the nonperturbative transition matrix element $\langle\Lambda|\,O_i\,|\Lambda_b\rangle$. Among the phenomenological models used are the bag model [2], a pole model [3, 4], the covariant oscillator quark model [5], nonrelativistic quark models [6, 7], a perturbative QCD approach using light–cone distribution amplitudes calculated from QCD sum rules [8]. The authors of [3, 4, 9–13] have made use of the heavy quark mass limit to write their form factors in terms of two independent heavy quark effective theory (HQET) form factors [14–16] for which they provide some estimates. Mannel and Recksiegel [3] and Colangelo et al. [4] use experimental input for this estimate, while [9–13] use QCD sum rules to determine the two HQET form factors. Recently the Λ_b rare decays were studied in lattice QCD [17] and used an improved version of the QCD sum rules [18].

As has been emphasized by [9, 19, 20] heavy quark symmetry should not be relied on at small q^2, i.e. close to maximal recoil, in particular for heavy–to–light transitions. Heavy quark symmetry is expected to be reliable close

* On leave of absence from Department of Physics, Tomsk State University, 634050 Tomsk, Russia

to zero recoil where not much momentum is transferred to the spectator system. As one moves away from the zero recoil point and more momentum gets transferred to the spectator system, hard gluon exchange including spin flip interactions become more important and the heavy quark symmetry can be expected to break down [19, 20]. One should, therefore, not rely on a form factor parametrization in terms of only two heavy quark symmetry form factors for the whole q^2 range as has been done in Refs. [3, 9–13].

Furthermore, the results of QCD sum rules for heavy–to–light transitions have been shown to be unreliable close to maximum recoil [21]. One should rather rely on light–cone sum rules for the near maximum recoil region for the evaluation of the hadronic form factors. It is for these reasons that most recent calculations have employed light–cone sum rules to calculate the whole set of hadronic form factors [22–32]. The form factors are then extrapolated to the low recoil region by using some pole–type parametrizations. The authors of [26–28] have derived some very interesting form factor relations in the large recoil region using soft collinear effective theory (SCET).

Apart from rates, q^2–spectra, lepton–side forward-backward asymmetries treated in most of the papers some of the authors have also discussed polarization effects of the final state particles. For example, in Refs. [3, 10, 11, 26] the polarization of the daughter baryon Λ was calculated which can be measured experimentally by analyzing the decay $\Lambda \to p\,\pi^-$. The polarization components of a single lepton have been considered in [11, 12] while the authors of Ref. [13] have even studied double–lepton polarization asymmetries. Polarization effects of the decaying Λ_b have been investigated in [29]. Non-Standard Model effects for various observables have been examined in Refs. [4, 9, 12, 13, 23, 24, 30–32].

There are large discrepancies in the predictions of the different models for the various observables, in particular for the photonic decay $\Lambda_b \to \Lambda\,\gamma$ and for the near–zero–recoil τ–mode $\Lambda_b \to \Lambda\,\tau^+\tau^-$. It will be interesting to compare the results of future experiments on rare baryon decays with the various model predictions, in particular for the above two decay modes.

In the present paper we use the covariant constituent quark model (for short: covariant quark model) as dynamical input to calculate the nonperturbative transition matrix elements. In the covariant quark model the current–induced transitions between baryons are calculated from two–loop Feynman diagrams with free quark propagators in which the divergent high energy behavior of the loop integrations is tempered by Gaussian vertex functions [33]-[43]. An attractive new feature has recently been added to the covariant quark model in as much as quark confinement has now been incorporated in an effective way, i.e. there are no quark thresholds and thus no free quarks in the relevant Feynman diagrams [44–46]. We emphasize that the covariant quark model described here is a truly frame–independent field–theoretic quark model in contrast to other constituent quark models which are basically quantum mechanical with built–in relativistic elements. One of the advantages of the covariant quark model is that it allows one to calculate the transition form factors in the full accessible range of q^2–values.

We somehow deviate from the traditional order when presenting our results. We first discuss the model independent aspects of the problem involving spin physics. This is done by use of the helicity amplitude method which leads to comprehensive, compact and clearly organized formulae for the joint angular decay distributions of the decay products and the spin density matrix elements of the final state particles. Lepton mass effects are automatically included. At a later stage we present the details of the dynamics for which we give numerical results towards the end of the paper. We believe that, in this paper, and in a forthcoming paper, we provide the first complete and comprehensive discussion of all the spin physics aspects of the decay $\Lambda_b \to \Lambda\,\ell^+\ell^-$.

We mention that our helicity formulae are ideally suited as input in an event generator. This has been previously demonstrated for the charged current decay $\Xi^0 \to \Sigma^+\ell^-\bar{\nu}_\ell$ $(\ell = e, \mu)$ followed by the decay $\Sigma^+ \to p\pi^0$ including even polarization effects for the Ξ^0 [47]. We have written a Monte Carlo (MC) event generator for the above process based on decay distribution formulae derived from a corresponding helicity analysis. The event generator is based on the *genbod* routine from the CERNLIB library and has been used by the NA48 experiment to analyze their data on the above process.

Our paper is structured as follows. In Sec. II, we present a detailed discussion of the helicity formalism that allows one to write down the joint angular distribution of the cascade decay $\Lambda_b \to \Lambda(\to p\pi^-) + j_{\rm eff}(\to \ell^+\ell^-)$. In Sec. III we review the basic notions of our dynamical approach — *the covariant quark model for baryons*. In particular, we i) derive the phenomenological Lagrangians describing the interaction of baryons with their constituent quarks ii) introduce the corresponding interpolating 3–quark currents with the quantum numbers of the respective baryon iii) discuss the idea and implementation of quark confinement iv) present the calculational loop integration techniques. In Sec. IV, we consider the application of our approach to the rare one-photon decay $\Lambda_b \to \Lambda\gamma$ and the dilepton decay $\Lambda_b \to \Lambda(\to p\pi^-) + j_{\rm eff}(\to \ell^+\ell^-)$. Finally, in Sec. V, we summarize our results. Some technical material has been relegated to the Appendices A–E.

II. JOINT ANGULAR DECAY DISTRIBUTION

As in the case of the rare meson decays $B \to K^{(*)}\ell^+\ell^-$ ($\ell = e, \mu, \tau$) treated in [48] one can exploit the cascade nature of the decay $\Lambda_b \to \Lambda(\to p\pi^-) + j_{\rm eff}(\to \ell^+\ell^-)$ to write down a joint angular decay distribution involving the polar angles θ, θ_B and the azimuthal angles χ defined by the decay products in their respective (center of mass) CM systems as shown in Fig.1. The angular decay distribution involves the helicity amplitudes $h^m_{\lambda_1\lambda_2}$ for the decay $j_{\rm eff} \to \ell^+\ell^-$, $H^m_{\lambda_\Lambda\lambda_j}$ for the decay $\Lambda_b \to \Lambda + j_{\rm eff}$ and $h^B_{\lambda_p 0}$ for the decay $\Lambda \to p + \pi^-$. The joint angular decay distribution for the decay of an unpolarized Λ_b reads

$$
\begin{aligned}
W(\theta,\theta_B,\chi) \;\propto\; & \sum_{\lambda_1,\lambda_2,\lambda_j,\lambda'_j,J,J',m,m',\lambda_\Lambda,\lambda'_\Lambda,\lambda_p} h^m_{\lambda_1\lambda_2}(J) h^{m'}_{\lambda_1\lambda_2}(J') e^{i(\lambda_j-\lambda'_j)\chi} \\
\times\; & \delta_{\lambda_j-\lambda_\Lambda,\lambda'_j-\lambda'_\Lambda}\delta_{JJ'} d^J_{\lambda_j,\lambda_1-\lambda_2}(\theta) d^{J'}_{\lambda'_j,\lambda_1-\lambda_2}(\theta) H^m_{\lambda_\Lambda\lambda_j}(J) H^{m'\dagger}_{\lambda'_\Lambda\lambda'_j}(J') \\
\times\; & d^{1/2}_{\lambda_\Lambda\lambda_p}(\theta_B) d^{1/2}_{\lambda'_\Lambda\lambda_p}(\theta_B) h^B_{\lambda_p 0} h^{B\,\dagger}_{\lambda_p 0}\,. \qquad (1)
\end{aligned}
$$

The Kronecker delta in $\delta_{\lambda_j-\lambda_\Lambda,\lambda'_j-\lambda'_\Lambda}$ in (1) expresses the fact that we are considering the decay of an unpolarized Λ_b. In Eq. (1) one has to observe that $|\lambda_j - \lambda_\Lambda| = |\lambda'_j - \lambda'_\Lambda| = 1/2$ due to the spin 1/2 nature of the decaying Λ_b. The corresponding Kronecker delta has not been included in (1) and will also be omitted in the subsequent formulas. The $d^j_{mm'}$ in Eq. (1) with ($j = 0, 1/2, 1$) are Wigner's d–functions where $d^0_{00} = 1$. In Appendix A we provide an explicit expression for the three-fold angular decay distribution by expanding out the r.h.s. of Eq. (1). We mention that it is not difficult to generalize Eq. (1) to the case of a decaying polarized Λ_b as has been done in [29] by transcribing the results of the corresponding semileptonic charged current decays [47, 49].

Let us discuss the helicity amplitudes appearing in Eq. (1) in turn. The lepton–side helicity amplitudes $h^m_{\lambda_1\lambda_2}$ for the process $j_{\rm eff} \to \ell^+\ell^-$ are defined by ($\hat\lambda_j = \lambda_1 - \lambda_2$)

$$
\begin{aligned}
m=1 \quad (V) \qquad & h^1_{\hat\lambda_j;\lambda_1\lambda_2}(J) \;=\; \bar u_2(\lambda_2)\,\gamma_\mu\, v_1(\lambda_1)\,\epsilon(\hat\lambda_j)\,, \\
m=2 \quad (A) \qquad & h^2_{\hat\lambda_j;\lambda_1\lambda_2}(J) \;=\; \bar u_2(\lambda_2)\,\gamma_\mu\gamma_5\, v_1(\lambda_1)\,\epsilon(\hat\lambda_j)\,. \qquad (2)
\end{aligned}
$$

We have put a hat on the helicity label $\hat\lambda_j$ to emphasize that $\hat\lambda_j$ is not the λ_j appearing in Eq. (1). We have also included the label ($\hat\lambda_j = \lambda_1 - \lambda_2$) in Eq. (2) for clarity even if the notation is redundant. We evaluate the helicity amplitudes in the ($\ell^+\ell^-$) CM system with ℓ^+ defining the z–direction. The label (J) takes the values ($J = 0$) with $\lambda_j = 0$ and ($J = 1$) with $\lambda_j = \pm1, 0$ for the scalar and vector parts of the effective current $j_{\rm eff}$, respectively. In order to distinguish between the two $\lambda_j = 0$ cases we write $\lambda_j = t$ for the ($J = 0$) scalar case and $\lambda_j = 0$ for the ($J = 1$) vector case. The lepton–side helicity amplitudes can be calculated to be

$$
\begin{aligned}
h^1_{t\,;\frac12\,\frac12}(J=0) &= 0\,, \\
h^1_{0\,;\frac12\,\frac12}(J=1) &= 2m_\ell\,, \\
h^1_{+1\,;\frac12\,-\frac12}(J=1) &= -\sqrt{2q^2}\,, \qquad (3)\\
h^2_{t;\frac12\,\frac12}(J=0) &= 2m_\ell\,, \\
h^2_{0;\frac12\,\frac12}(J=1) &= 0\,, \\
h^2_{+1;\frac12\,-\frac12}(J=1) &= \sqrt{2q^2}\;\; v\,.
\end{aligned}
$$

where $v = \sqrt{1 - 4m_\ell^2/q^2}$ is the lepton velocity in the ($\ell^+\ell^-$) CM frame and m_ℓ is the leptonic mass.

From parity one has

$$
\begin{aligned}
h^1_{-\lambda_j;-\lambda_1-\lambda_2} &= h^1_{\lambda_j;\lambda_1\lambda_2}\,, \qquad (4)\\
h^2_{-\lambda_j;-\lambda_1-\lambda_2} &= -\,h^2_{\lambda_j;\lambda_1\lambda_2}\,.
\end{aligned}
$$

In Eq. (1) we are summing over the lepton helicities. A closer look at the relations (3,4) shows that there are no ($J = 0; J = 1$) interference effects in the joint angular decay distribution (1). This has been annotated by the Kronecker delta $\delta_{JJ'}$ in (1). ($J = 0; J = 1$) interference effects come into play when one leaves the lepton helicities unsummed, i.e. when one considers lepton polarization effects. In this case one has to replace $\delta_{JJ'}$ by $(-1)^{J+J'}$ in

Eq. (1) where the extra minus sign for the $(J = 0; J = 1)$ interference contribution results from the Minkowskian form of the metric tensor [47, 49, 50]. We mention that $(J = 0; J = 1)$ interference effects occur in charged current transitions already in the unpolarized lepton case [47, 49, 50].

From Eq. (3) it is clear that the scalar contributions enter the game only for nonzero lepton masses $m_\ell \neq 0$. The scalar contributions will thus only be important for the τ–mode.

The hadronic helicity amplitudes $H^m_{\lambda_\Lambda \lambda_j}(J)$ in Eq. (1) describe the full dynamics of the current–induced transitions $\Lambda_b \to \Lambda + j_{\rm eff}$ including the structure and the values of the short distance coefficients of the pertinent penguin operators. The helicity labels on the helicity amplitudes $H^m_{\lambda_\Lambda \lambda_j}(J)$ take the values $\lambda_\Lambda = \pm\frac{1}{2}$, $\lambda_j = t$ for $(J = 0)$ and $\lambda_j = \pm 1, 0$ for $(J = 1)$ as described above. The superscript m on $H^m_{\lambda_\Lambda \lambda_j}(J)$ defines whether the hadronic helicity amplitude multiplies the lepton vector current $\bar{u}(\ell^-)\gamma_\mu\, v(\ell^+)$ $(m = 1)$ or the axial vector current $\bar{u}(\ell^-)\gamma_\mu\gamma_5\, v(\ell^+)$ $(m = 2)$. More details on the definitions of the hadronic helicity amplitudes and their calculation in the covariant quark model can be found in Sec. III.

If desired one can switch from the helicity amplitudes used here to the transversity amplitudes used e.g. in [51] by use of the relations

$$A^m_{\lambda_\Lambda \perp,\parallel} = (H^m_{\lambda_\Lambda +1} \mp H^m_{\lambda_\Lambda -1})/\sqrt{2}, \quad A^m_{\lambda_\Lambda 0} = H^m_{\lambda_\Lambda 0}\,, \quad A^m_{\lambda_\Lambda t} = H^m_{\lambda_\Lambda t}\,. \tag{5}$$

The advantage of the transversity amplitudes is that they have definite transformation properties under parity.

The helicity amplitudes $h^B_{\lambda_p \lambda_\pi = 0}$, finally, describe the decay $\Lambda \to p + \pi^-$. We shall use experimental input for the relevant bilinear forms of the helicity amplitudes. The helicity labels on the helicity amplitudes $h^B_{\lambda_p \lambda_\pi = 0}$ are self–explanatory.

As mentioned in the introduction the joint angular decay distribution Eq. (1) is ideally suited as input to an event generator using sequential boosts to the respective rest systems of the secondary particles as exemplified by the cascade–type decay distribution (1).

We mention that the decay distribution Eq. (1) reproduces the results in Ref. [48] for $B \to K^{(*)}(\to K\pi)\ell^+\ell^-$ when one replaces the helicity amplitudes for $\Lambda \to p + \pi^-$ by the corresponding helicity amplitude for $K^* \to K\pi$. The necessary replacement is

$$H^m_{\lambda_\Lambda \lambda_j} H^{m'\dagger}_{\lambda'_\Lambda \lambda'_j} d^{1/2}_{\lambda_\Lambda \lambda_p}(\theta_B) d^{1/2}_{\lambda'_\Lambda \lambda_p}(\theta_B) h^B_{\lambda_p 0} h^{B\,\dagger}_{\lambda_p 0} \quad \to \quad H^m_{\lambda_{K^*} \lambda_j} H^{m'\dagger}_{\lambda'_{K^*} \lambda'_j} d^1_{0\,\lambda_j}(\theta^*) d^1_{0\,\lambda'_j}(\theta^*) h^{K^*}_{00} h^{K^*\dagger}_{00} \tag{6}$$

where, in the mesonic case, $\lambda_{K^*} = -\lambda_j$ and $\lambda'_{K^*} = -\lambda'_j$ since the decaying B has spin zero. In Eq. (6) we have omitted the label (J) on the hadronic helicity amplitudes for brevity. Note that there is only one helicity amplitude for $K^* \to K\pi$ compared to the two helicity amplitudes for $\Lambda \to p + \pi^-$. A new feature of the baryonic case is that the decay $\Lambda \to p + \pi^-$ is parity nonconserving which leads to a forward–backward asymmetry on the hadron side as is the case on the lepton side.

In this paper we will not further consider the azimuthal χ–dependence of the joint angular decay distribution Eq. (1) but we shall rather integrate (1) over the azimuthal angle χ. This leads to $\lambda_j = \lambda'_j$ via $\int_0^{2\pi} d\chi \exp[\,i(\lambda_j - \lambda'_j)\,\chi] = 2\pi\,\delta_{\lambda_j \lambda'_j}$. Since we are considering the decay of an unpolarized Λ_b such that $\lambda_{\Lambda_b} = \lambda'_{\Lambda_b}$ one also has the equality $\lambda_\Lambda = \lambda'_\Lambda$ after azimuthal integration due to the fact that $\lambda_{\Lambda_b} = \lambda_j - \lambda_\Lambda$ and $\lambda'_{\Lambda_b} = \lambda_j - \lambda'_\Lambda$. One then obtains the two–fold angular decay distribution

$$\begin{aligned} W(\theta,\theta_B) \;\propto\; & 2\pi \sum_{\lambda_1,\lambda_2,\lambda_j,J,m,m',\lambda_\Lambda,\lambda_p} h^m_{\lambda_1\lambda_2}(J) h^{m'}_{\lambda_1\lambda_2}(J) \\ & \times\; d^J_{\lambda_j,\lambda_1-\lambda_2}(\theta) d^J_{\lambda_j,\lambda_1-\lambda_2}(\theta) H^m_{\lambda_\Lambda\lambda_j}(J) H^{m'\dagger}_{\lambda_\Lambda\lambda_j}(J) \\ & \times\; d^{1/2}_{\lambda_\Lambda\lambda_p}(\theta_B) d^{1/2}_{\lambda_\Lambda\lambda_p}(\theta_B) h^B_{\lambda_p 0} h^{B\,\dagger}_{\lambda_p 0}\,. \end{aligned} \tag{7}$$

The fact that $\lambda_\Lambda = \lambda'_\Lambda$ in (7) implies that the spin density matrix of the daughter baryon Λ appearing in (7) is purely diagonal implying that in a polar angle analysis such as the one in Eq. (7) one can only probe the longitudinal polarization P^Λ_z of the Λ.

In Eq. (1) we have summed over the helicity labels of the leptons, i.e. we have taken the trace of the respective spin density matrices. By leaving the respective helicity labels unsummed one can then obtain single lepton and double lepton spin asymmetries as have been discussed in Refs. [11] and [13], respectively. As mentioned before one can treat the decay of a polarized Λ_b in a similar vein.

In the following subsections we will consider various integrated forms of Eq. (7).

A. Differential rate

The differential rate is obtained from the two–fold angular decay distribution Eq. (7) by integrations over $(\cos\theta_B, \cos\theta)$. For the $\cos\theta_B$– integration one uses $\int_{-1}^{1} d\cos\theta_B d^{1/2}_{\lambda_\Lambda\lambda_p}(\theta_B) d^{1/2}_{\lambda_\Lambda\lambda_p}(\theta_B) = 1$. The $\cos\theta$– integration, finally, can be done by using $\int_{-1}^{1} d\cos\theta\, d^J_{\lambda_j,\lambda_1-\lambda_2}(\theta) d^J_{\lambda_j,\lambda_1-\lambda_2}(\theta) = 2/3$ for $J=1$, and 2 for $J=0$. One obtains

$$
\begin{aligned}
W \;\propto\; & \tfrac{2}{3}\cdot 2\pi \cdot \sum_{\lambda_1,\lambda_2,\lambda_j,J,m,\lambda_\Lambda} h^m_{\lambda_1\lambda_2}(J) h^m_{\lambda_1\lambda_2}(J) \\
\times\; & (3\,\delta_{J\,0} + \delta_{J\,1}) H^m_{\lambda_\Lambda\lambda_j}(J) H^{\dagger m}_{\lambda_\Lambda\lambda_j}(J) \sum_{\lambda_p} h^B_{\lambda_p 0} h^{B\,\dagger}_{\lambda_p 0}\,.
\end{aligned} \tag{8}
$$

Note that the differential rate obtains only parity conserving diagonal contributions such that $m = m'$.

Let us define rate functions $\Gamma^{mm'}_X$ $(X = U, L, S)$ through

$$
\frac{d\Gamma^{mm'}_X}{dq^2} = \frac{1}{2}\frac{G_F^2}{(2\pi)^3}\left(\frac{\alpha|\lambda_t|}{2\pi}\right)^2 \frac{|\mathbf{p_2}|\, q^2\, v}{12\, M_1^2}\, H^{mm'}_X\,, \tag{9}
$$

where $\alpha = 1/137.036$ is the fine structure constant, $G_F = 1.16637\times 10^{-5}$ GeV^{-2} is the Fermi coupling constant, $\lambda_t = V^\dagger_{ts} V_{tb} = 0.041$ is the product of corresponding Kabayashi-Maskawa matrix elements and $|\mathbf{p_2}| = \lambda^{1/2}(M_1^2, M_2^2, q^2)/2M_1$ is the momentum of the Λ-hyperon in the Λ_b-rest frame. Note that we have included the statistical factor $1/(2S_{\Lambda_b}+1) = 1/2$ in the definition of the rate functions.

The bilinear expressions $H^{mm'}_X$ $(X = U, L, S)$ are defined by

$$
\begin{aligned}
H^{mm'}_U &= \mathrm{Re}(H^m_{\frac{1}{2}1} H^{\dagger m'}_{\frac{1}{2}1}) + \mathrm{Re}(H^m_{-\frac{1}{2}-1} H^{\dagger m'}_{-\frac{1}{2}-1}) \quad \text{unpolarized-transverse}\,,\\
H^{mm'}_L &= \mathrm{Re}(H^m_{\frac{1}{2}0} H^{\dagger m'}_{\frac{1}{2}0}) + \mathrm{Re}(H^m_{-\frac{1}{2}0} H^{\dagger m'}_{-\frac{1}{2}0}) \quad \text{longitudinal}\,,\\
H^{mm'}_S &= \mathrm{Re}(H^m_{\frac{1}{2}t} H^{\dagger m'}_{\frac{1}{2}t}) + \mathrm{Re}(H^m_{-\frac{1}{2}t} H^{\dagger m'}_{-\frac{1}{2}t}) \quad \text{scalar}\,.
\end{aligned} \tag{10}
$$

Note that, compared to [48], we have redefined the scalar structure function $H^{mm'}_S$ by omitting a factor of 3 in the definition of the scalar structure function.

Putting in the correct normalization factors one obtains the differential rate $d\Gamma/dq^2$ which reads

$$
\frac{d\Gamma(\Lambda_b \to \Lambda\,\ell^+\ell^-)}{dq^2} = \frac{v^2}{2}\cdot\left(U^{11+22} + L^{11+22}\right) + \frac{2m_\ell^2}{q^2}\cdot\frac{3}{2}\cdot\left(U^{11} + L^{11} + S^{22}\right), \tag{11}
$$

where we have adopted the notations $d\Gamma^{mm'}_X/dq^2 = X^{mm'}$ and $X^{11+22} = X^{11} + X^{22}$. Here, and in the following, we do an importance sampling of our rate expressions by sorting the contributions according to powers of the threshold factor v. When one wants to compare our results to the corresponding results for the mesonic case written down in Ref. [48] one has to rearrange the contributions in Ref. [48] accordingly. And, one has to take into account the factor of 3 difference in the definition of the scalar structure function. We mention that the authors of [51] have also written their mesonic decay distributions in terms of powers of the threshold factor v. The second term proportional to $2m_\ell^2/q^2$ in (11) can be seen to arise from the s–wave contributions to $\ell^+\ell^-$ production: $(J=1)$ in U^{11} and L^{11} associated with the vector current $m=1$, and $(J=0)$ in S^{22} associated with the axial vector current $m=2$ (see Eq. (3)).

The total rate, finally, is obtained by q^2–integration in the range

$$
4m_\ell^2 \;\le\; q^2 \;\le\; (M_1 - M_2)^2\,. \tag{12}
$$

For the lower q^2 limit one has $4m_\ell^2 = (1.04\times 10^{-6}, 0.045, 12.6284)$ GeV^2 for $\ell = (e, \mu, \tau)$. The upper limit of the q^2–integration is given by $(M_{\Lambda_b} - M_\Lambda)^2 = 20.29$ GeV^2. For $\ell = (e,\mu)$ one is practically probing the whole q^2 region while for $\ell = \tau$ the q^2–range is restricted to the low recoil half of phase-space starting at $\sqrt{q^2} = 3.55$ GeV just below the position of the $\Psi(2S)$ vector meson resonance.

B. Lepton–side decay distribution

Integrating the two–fold decay distribution (7) over $\cos\theta_B$ one obtains

$$W(\theta) \;\propto\; 2\pi \sum_{\lambda_1,\lambda_2,\lambda_j,J,m,m',\lambda_\Lambda} h^m_{\lambda_1\lambda_2}(J) h^{m'}_{\lambda_1\lambda_2}(J)$$
$$d^J_{\lambda_j,\lambda_1-\lambda_2}(\theta) d^J_{\lambda_j,\lambda_1-\lambda_2}(\theta) H^m_{\lambda_\Lambda\lambda_j}(J) H^{\dagger m'}_{\lambda_\Lambda\lambda_j}(J) \;\sum_{\lambda_p} h^B_{\lambda_p 0} h^{B\,\dagger}_{\lambda_p 0}\,. \tag{13}$$

The lepton–side decay distribution involves one more parity–odd structure function which is defined by

$$H_P^{mm'} = \mathrm{Re}(H^m_{\frac12 1} H^{\dagger m'}_{\frac12 1}) - \mathrm{Re}(H^m_{-\frac12 -1} H^{\dagger m'}_{-\frac12 -1}) \quad \text{parity–odd} \tag{14}$$

Putting in the correct normalization one obtains

$$\frac{d\Gamma(\Lambda_b \to \Lambda\,\ell^+\ell^-)}{dq^2 d\cos\theta} \;=\; v^2 \cdot \left[\frac38 (1+\cos^2\theta)\cdot \frac12 U^{11+22} \;+\; \frac34 \sin^2\theta \cdot \frac12 L^{11+22}\right]$$
$$-\;\; v\cdot \frac34 \cos\theta \cdot P^{12} \;+\; \frac{2m_\ell^2}{q^2}\cdot\frac34\cdot\left[U^{11}+L^{11}+S^{22}\right]. \tag{15}$$

One can define a lepton–side forward–backward asymmetry A^ℓ_{FB} by $A^\ell_{FB} = (F-B)/(F+B)$ where F and B denote the rates in the forward and backward hemispheres

$$A^\ell_{FB}(q^2) = -\frac32 \,\frac{v\cdot P^{12}}{v^2\cdot\left(U^{11+22}+L^{11+22}\right) + \frac{2m_\ell^2}{q^2}\cdot 3\cdot\left(U^{11}+L^{11}+S^{22}\right)}\,. \tag{16}$$

Note that the lepton–side forward–backward asymmetry vanishes at threshold $q^2 \to 4m_\ell^2$. The integrated forward–backward asymmetry is defined as

$$\bar{A}^\ell_{FB} = -\frac32 \,\frac{\int\limits_{4m_\ell^2}^{(M_1-M_2)^2} dq^2\,\left(v\cdot P^{12}\right)}{\int\limits_{4m_\ell^2}^{(M_1-M_2)^2} dq^2 \left(v^2\cdot\left(U^{11+22}+L^{11+22}\right)+\frac{2m_\ell^2}{q^2}\cdot 3\cdot\left(U^{11}+L^{11}+S^{22}\right)\right)}\,. \tag{17}$$

C. Λ–polarization and hadron–side decay distribution

Integrating the two–fold decay distribution (7) over $\cos\theta$ one obtains

$$W(\theta_B) \;\propto\; \tfrac23\cdot 2\pi\cdot \sum_{\lambda_1,\lambda_2,\lambda_j,J,m,m',\lambda_\Lambda,\lambda_p} h^m_{\lambda_1\lambda_2}(J) h^{m'}_{\lambda_1\lambda_2}(J)$$
$$\times\;\; (\delta_{J\,1}+3\,\delta_{J\,0}) H^m_{\lambda_\Lambda\lambda_j}(J) H^{\dagger m'}_{\lambda_\Lambda\lambda_j}(J)\; d^{1/2}_{\lambda_\Lambda\lambda_p}(\theta_B) d^{1/2}_{\lambda_\Lambda\lambda_p}(\theta_B) h^B_{\lambda_p 0} h^{B\,\dagger}_{\lambda_p 0}\,. \tag{18}$$

In fact, one finds from the structure of the lepton helicity amplitudes Eq. (3) and (4) that only $(m=m')$ contributions survive in Eq. (18).

By chopping off the $\Lambda \to p\pi$ decay structure $d^{1/2}_{\lambda_\Lambda\lambda_p}(\theta_B) d^{1/2}_{\lambda_\Lambda\lambda_p}(\theta_B) h^B_{\lambda_p 0} h^{B\,\dagger}_{\lambda_p 0}$ and leaving the helicity λ_Λ of the Λ unsummed one obtains the diagonal spin density matrix of the Λ given by

$$W_{\lambda_\Lambda\lambda_\Lambda} \propto \tfrac23\cdot 2\pi\cdot \sum_{\lambda_1,\lambda_2,\lambda_j,J,m} h^m_{\lambda_1\lambda_2}(J) h^m_{\lambda_1\lambda_2}(J) (\delta_{J\,1}+3\,\delta_{J\,0}) H^m_{\lambda_\Lambda\lambda_j}(J) H^{\dagger m}_{\lambda_\Lambda\lambda_j}(J)\,. \tag{19}$$

The z–component of the polarization of the daughter baryon Λ can then be calculated from the diagonal spin density matrix elements according to

$$P_z^\Lambda = \frac{W_{\frac12\frac12} - W_{-\frac12 -\frac12}}{W_{\frac12\frac12} + W_{-\frac12 -\frac12}}\,, \tag{20}$$

which gives

$$P_z^\Lambda = \frac{v^2 \cdot \big(P^{11+22} + L_P^{11+22} \big) + \frac{2m_\ell^2}{q^2} \cdot 3 \cdot \big(P^{11} + L_P^{11} + S_P^{22} \big)}{v^2 \cdot \big(U^{11+22} + L^{11+22} \big) + \frac{2m_\ell^2}{q^2} \cdot 3 \cdot \big(U^{11} + L^{11} + S^{22} \big)} \,. \tag{21}$$

One has to keep in mind that $X^{mm'}$ stands for the differential expression $d\Gamma_X^{mm'}/dq^2$ ($X = U, L, S, P, L_P, S_P$). When averaging the polarization P_z^Λ over q^2 one has to remember to separately average the numerator and denominator in (21).

In (21) we have defined two new parity–violating structure functions according to

$$\begin{aligned} H_{L_P}^{mm'} &= \mathrm{Re}(H^m_{\frac{1}{2}0} H^{\dagger m'}_{\frac{1}{2}0} - H^m_{-\frac{1}{2}0} H^{\dagger m'}_{-\frac{1}{2}0}) \quad \text{longitudinal–polarized}\,, \\ H_{S_P}^{mm'} &= \mathrm{Re}(H^m_{\frac{1}{2}t} H^{\dagger m'}_{\frac{1}{2}t} - H^m_{-\frac{1}{2}t} H^{\dagger m'}_{-\frac{1}{2}t}) \quad \text{scalar–polarized}\,. \end{aligned} \tag{22}$$

Returning to Eq. (18) we write down the correctly normalized single–angle decay distribution which reads

$$\begin{aligned} \frac{d\Gamma(\Lambda_b \to \Lambda(\to p\pi^-)\ell^+\ell^-)}{dq^2\, d\cos\theta_B} &= \mathrm{Br}(\Lambda \to p\pi^-) \\ &\times \frac{1}{2}\bigg\{ \frac{v^2}{2} \cdot \Big[U^{11+22} + L^{11+22} + \Big(P^{11+22} + L_P^{11+22} \Big) \alpha_B \cos\theta_B \Big] \\ &+ \frac{2m_\ell^2}{q^2} \cdot \frac{3}{2} \cdot \Big[U^{11} + L^{11} + S^{22} + \Big(P^{11} + L_P^{22} + S_P^{22} \Big) \alpha_B \cos\theta_B \Big] \bigg\} \,, \end{aligned} \tag{23}$$

which, using the rate Eq. (15) and the polarization (21), can be rewritten as

$$\frac{d\Gamma(\Lambda_b \to \Lambda(\to p\pi^-)\ell^+\ell^-)}{dq^2\, d\cos\theta_B} = \mathrm{Br}(\Lambda \to p\pi^-) \frac{1}{2} \frac{d\Gamma(\Lambda_b \to \Lambda\, \ell^+\ell^-)}{dq^2} \Big(1 + \alpha_B P_z^\Lambda \cos\theta_B \Big) \,. \tag{24}$$

In Eqs. (23) and (24) we have made use of the asymmetry parameter α_B in the decay $\Lambda \to p + \pi^-$ which is defined by

$$\alpha_B = \frac{|h^B_{\frac{1}{2}0}|^2 - |h^B_{-\frac{1}{2}0}|^2}{|h^B_{\frac{1}{2}0}|^2 + |h^B_{-\frac{1}{2}0}|^2} \,. \tag{25}$$

The asymmetry parameter has been measured to be $\alpha_B = 0.642 \pm 0.013$ [52]. As a check on (23) one recovers the differential rate expression Eq. (8) by integrating over $\cos\theta_B$ and removing the factor $\mathrm{Br}(\Lambda \to p\pi^-)$.

Corresponding to the lepton–side forward–backward asymmetry A_{FB}^ℓ one can define a hadron–side forward–backward asymmetry A_{FB}^h defined by $A_{FB}^h = (F - B)/(F + B)$. Contrary to the mesonic case $B \to K^*(\to K\pi) + \ell^+\ell^-$ the hadron–side forward–backward asymmetry in $\Lambda_b \to \Lambda\ell^+\ell^-$ is nonzero since the decay $\Lambda \to p + \pi^-$ is parity nonconserving, i.e. one has $h^B_{\frac{1}{2}0} \neq h^B_{-\frac{1}{2}0}$ with 64% analyzing power. Using the form Eq. (24) one finds that the forward–backward asymmetry is simply related to the polarization P_z^Λ via

$$A_{FB}^h(q^2) = \frac{\alpha_B}{2} P_z^\Lambda(q^2) \,. \tag{26}$$

The integrated forward–backward asymmetry is defined as

$$\bar{A}_{FB}^h = \frac{\alpha_B}{2} \frac{\int\limits_{4m_\ell^2}^{(M_1-M_2)^2} dq^2 \left(v^2 \cdot \big(P^{11+22} + L_P^{11+22} \big) + \frac{2m_\ell^2}{q^2} \cdot 3 \cdot \big(P^{11} + L_P^{11} + S_P^{22} \big) \right)}{\int\limits_{4m_\ell^2}^{(M_1-M_2)^2} dq^2 \left(v^2 \cdot \big(U^{11+22} + L^{11+22} \big) + \frac{2m_\ell^2}{q^2} \cdot 3 \cdot \big(U^{11} + L^{11} + S^{22} \big) \right)} \,. \tag{27}$$

For the sake of completeness let us also list the θ_B–dependence of the polarization $P_z^\Lambda(\theta_B)$ which is obtained by chopping off the $\Lambda \to p\pi$ decay structure in Eq. (7) and proceeding as before when calculating the $\cos\theta_B$–independent polarization (21). One obtains

$$P_z^\Lambda(q^2,\theta_B) = \frac{v^2\left(\frac{3}{8}(1+\cos^2\theta_B)\cdot P^{11+22} + \frac{3}{2}\sin^2\theta_B\cdot L_P^{11+22}\right) - v\,\frac{3}{2}\cos\theta_B\cdot U^{12} + \frac{2m_\ell^2}{q^2}\cdot\frac{3}{2}\cdot\left(P^{11}+L_P^{11}+S_P^{22}\right)}{v^2\left(\frac{3}{8}(1+\cos^2\theta_B)\cdot U^{11+22} + \frac{3}{2}\sin^2\theta_B\cdot L^{11+22}\right) - v\,\frac{3}{2}\cos\theta_B\cdot P^{12} + \frac{2m_\ell^2}{q^2}\cdot\frac{3}{2}\cdot\left(U^{11}+L^{11}+S^{22}\right)}\,. \tag{28}$$

In this section we have only discussed the z–component of the polarization of the daughter baryon Λ. As mentioned before the contribution of the transverse polarization component P_x^Λ (as e.g. calculated in [9]) averages out after χ–integration since it enters the angular decay distribution with an angular factor $\propto P_x^\Lambda \alpha_B \cos\chi \sin\theta_B$ (see Eq. (1) or Ref. [47]).

III. Λ-TYPE BARYONS IN THE THE COVARIANT QUARK MODEL

In this section we discuss the basic ingredients of the covariant quark model which will be used for the calculation of the rare decays of Λ_b baryon. A detailed description of baryons as bound states of three quarks can be found in Refs. [39, 41–43, 45]. This includes a description of the structure of the Gaussian vertex factor, the choice of interpolating baryon currents as well as the compositeness condition for baryons.

The new features introduced to the meson sector in Refs. [44, 46] and applied to the baryon sector in Ref. [45] are both technical and conceptual. Instead of using Feynman parameters for the evaluation of the two–loop baryonic quark model Feynman diagram we now use Schwinger parameters. The technical advantage is that this leads to a simplification of the tensor loop integrations in as much as the loop momenta occurring in the quark propagators can be written as derivative operators. Furthermore, the use of Schwinger parameters allows one to incorporate quark confinement in an effective way. Details of these two new features of the covariant quark model have been described in [44–46].

In the following we consider $\Lambda = (Q[ud])$-type baryons needed in the present application. They consist of a heavy quark and two light quarks in a ${}^1S_0$ spin 0 configuration. The coupling of a Λ-type baryon to its constituent quarks is described by the Lagrangian

$$\mathcal{L}_{\rm int}^\Lambda(x) = g_\Lambda\,\bar\Lambda(x)\cdot J_\Lambda(x) + g_\Lambda\,\bar J_\Lambda(x)\cdot\Lambda(x)\,, \tag{29}$$

where we make use of the same $J_\Lambda(\bar J_\Lambda)$ interpolating three quark current for all three Λ-type baryons.

In general, for the Λ-type baryons one can construct three types of currents without derivatives — pseudoscalar J^P, scalar J^S and axial-vector J^A (see, Refs. [34, 38, 39, 43]):

$$\begin{aligned} J^P_{\Lambda_{Q[ud]}} &= \epsilon^{a_1a_2a_3}\,Q^{a_1}\,u^{a_2}C\gamma_5 d^{a_3}\,,\\ J^S_{\Lambda_{Q[ud]}} &= \epsilon^{a_1a_2a_3}\,\gamma^5\,Q^{a_1}\,u^{a_2}C d^{a_3}\,,\\ J^A_{\Lambda_{Q[ud]}} &= \epsilon^{a_1a_2a_3}\,\gamma^\mu\,Q^{a_1}\,u^{a_2}C\gamma_5\gamma_\mu d^{a_3}\,. \end{aligned} \tag{30}$$

The symbol $[ud]$ in the suffixes of the currents denote antisymmetrization of flavor and spin indices with respect to the light quarks u and d. We will consider the three flavor types of the Λ-baryons: $\Lambda_s^0(sud)$, $\Lambda_c^+(cud)$ and $\Lambda_b^0(bud)$. In Ref. [42] we have shown that, in the nonrelativistic limit, the J^P and J^A interpolating currents of the $\Lambda_{Q[ud]}$ baryons become degenerate and attain the correct nonrelativistic limit (in the case of single-heavy baryons this limit coincides with the heavy quark limit), while the J^S current vanishes in the nonrelativistic limit. On the other hand, the J^P and J^A interpolating currents of the Λ-type baryons become degenerate with SU($\mathrm{N_f}$)-symmetric currents. In Ref. [34] we have shown that, in the case of the heavy-to-light baryon transition $\Lambda_c^+ \to \Lambda^0 e^+\nu_e$, the use of a SU(3) symmetric Λ^0 hyperon is essential in order to describe data on $\Gamma(\Lambda_c^+ \to \Lambda^0 e^+\nu_e)$ (see also discussion in Refs. [6, 53]). In Appendix B we explicitly demonstrate that our J^P and J^A are degenerate with the SU($\mathrm{N_f}$)-symmetric currents. Therefore, in the following we restrict ourselves to the simplest pseudoscalar J^P current. The nonlocal interpolating three–quark current is written as

$$J_\Lambda(x) \;=\; \int\!\! dx_1\!\int\!\! dx_2\!\int\!\! dx_3\, F_\Lambda(x;x_1,x_2,x_3)\, J^{(\Lambda)}_{3q}(x_1,x_2,x_3)\,, \tag{31}$$
$$J^{(\Lambda)}_{3q}(x_1,x_2,x_3) \;=\; \tfrac{1}{2}\epsilon^{a_1a_2a_3}\, Q^{a_1}(x_1)\,\big(u^{a_2}(x_2)\, C\,\gamma^5\, d^{a_3}(x_3) - d^{a_2}(x_3)\, C\,\gamma^5\, u^{a_3}(x_2)\big)$$
$$\;=\; \epsilon^{a_1a_2a_3}\, Q^{a_1}(x_1)\, u^{a_2}(x_2)\, C\,\gamma^5\, d^{a_3}(x_3)\,,$$

$$\bar J_\Lambda(x) \;=\; \int\!\! dx_1\!\int\!\! dx_2\!\int\!\! dx_3\, F_\Lambda(x;x_1,x_2,x_3)\, \bar J^{(\Lambda)}_{3q}(x_1,x_2,x_3)\,,$$
$$\bar J^{(\Lambda)}_{3q}(x_1,x_2,x_3) \;=\; \epsilon^{a_1a_2a_3}\, \bar d^{a_3}(x_3)\,\gamma^5\, C\, \bar u^{a_2}(x_2)\cdot \bar Q^{a_1}(x_1)\,,$$

where $Q = s,c,b$. Here the matrix $C=\gamma^0\gamma^2$ is the usual charge conjugation matrix and the a_i $(i=1,2,3)$ are color indices.

The vertex function F_Λ characterizes the finite size of the Λ-type baryon. We assume that the vertex function is real. To satisfy translational invariance the function F_N has to fulfill the identity

$$F_\Lambda(x+a;x_1+a,x_2+a,x_3+a) \;=\; F_\Lambda(x;x_1,x_2,x_3) \tag{32}$$

for any given four-vector a. In the following we use a particular form for the vertex function

$$F_\Lambda(x;x_1,x_2,x_3) \;=\; \delta^{(4)}(x-\sum_{i=1}^{3} w_i x_i)\; \Phi_\Lambda\Big(\sum_{i<j}(x_i-x_j)^2\Big) \tag{33}$$

where Φ_Λ is the correlation function of the three constituent quarks with the coordinates x_1, x_2, x_3 and masses m_1, m_2, m_3, respectively. The variable w_i is defined by $w_i = m_i/(m_1+m_2+m_3)$ such that $\sum_{i=1}^3 w_i = 1$.

We shall make use of the Jacobi coordinates $\rho_{1,2}$ and the CM coordinate x which are defined by

$$\begin{aligned}
x_1 &= x + \tfrac{1}{\sqrt2}\, w_3\, \rho_1 - \tfrac{1}{\sqrt6}\,(2w_2+w_3)\,\rho_2\,,\\
x_2 &= x + \tfrac{1}{\sqrt2}\, w_3\, \rho_1 + \tfrac{1}{\sqrt6}\,(2w_1+w_3)\,\rho_2\,,\\
x_3 &= x - \tfrac{1}{\sqrt2}\,(w_1+w_2)\,\rho_1 + \tfrac{1}{\sqrt6}\,(w_1-w_2)\,\rho_2\,.
\end{aligned} \tag{34}$$

The CM coordinate is given by $x = \sum_{i=1}^3 w_i x_i$. In terms of the Jacobi coordinates one obtains

$$\sum_{i<j}(x_i-x_j)^2 = \rho_1^2+\rho_2^2\,. \tag{35}$$

Note that the choice of Jacobi coordinates is not unique. By using the particular choice of Jacobi coordinates given by Eq. (34) one obtains the following representation for the correlation function Φ_Λ in Eq. (33)

$$\Phi_\Lambda\Big(\sum_{i<j}(x_i-x_j)^2\Big) \;=\; \int\frac{d^4p_1}{(2\pi)^4}\int\frac{d^4p_2}{(2\pi)^4}\, e^{-ip_1(x_1-x_3)-ip_2(x_2-x_3)}\,\bar\Phi_\Lambda(-P_1^2-P_2^2)\,, \tag{36}$$
$$\bar\Phi_\Lambda(-P_1^2-P_2^2) \;=\; \tfrac{1}{9}\int d^4\rho_1\int d^4\rho_2\, e^{iP_1\rho_1+iP_2\rho_2}\,\Phi_\Lambda(\rho_1^2+\rho_2^2)\,,$$
$$P_1 = \tfrac{1}{\sqrt2}(p_1+p_2)\,, \qquad P_2 = -\tfrac{1}{\sqrt6}(p_1-p_2)\,.$$

This representation is valid for any choice of the set of Jacobi coordinates. The particular choice (34) is a preferred choice since it leads to the specific form of the argument $-P_1^2-P_2^2 = -\frac{2}{3}(p_1^2+p_2^2+p_1p_2)$. Since this expression is invariant under the transformations: $p_1\leftrightarrow p_2$, $p_2\to -p_2-p_1$ and $p_1\to -p_1-p_2$, the r.h.s. in Eq. (36) is invariant under permutations of all x_i as it should be.

In the next step we have to specify the function $\bar\Phi_\Lambda(-P_1^2-P_2^2)\equiv\bar\Phi_\Lambda(-P^2)$ which characterizes the finite size of the baryons. We will choose a simple Gaussian form for the function $\bar\Phi_\Lambda$:

$$\bar\Phi_\Lambda(-P^2) = \exp(P^{\,2}/\Lambda_\Lambda^2)\,, \tag{37}$$

where Λ_Λ is a size parameter parametrizing the distribution of quarks inside a Λ-type baryon. We use different values of the Λ_Λ parameter for different types of the Λ-type baryon: Λ_{Λ_s}, Λ_{Λ_c} and Λ_{Λ_b} for the Λ, Λ_c and Λ_b baryons, respectively. One has to note that we have used another definition of the Λ_Λ in our previous papers: $\Lambda_\Lambda = \Lambda_\Lambda^{\rm old}/(3\sqrt{2})$.

Since P^2 turns into $-P_E^2$ in Euclidean space the form (37) has the appropriate falloff behavior in the Euclidean region. We emphasize that any choice for Φ_Λ is appropriate as long as it falls off sufficiently fast in the ultraviolet region of Euclidean space to render the corresponding Feynman diagrams ultraviolet finite. The choice of a Gaussian form for Φ_Λ has obvious calculational advantages.

The coupling constants g_Λ are determined by the compositeness condition suggested by Weinberg [54] and Salam [55] (for review, see Ref. [56]) and extensively used in our approach (for details, see Ref. [57]). The compositeness condition in the case of baryons implies that the renormalization constant of the baryon wave function is set equal to zero:

$$Z_\Lambda = 1 - \Sigma_\Lambda^\prime(m_\Lambda) = 0 \tag{38}$$

where $\Sigma_\Lambda^\prime$ is the on-shell derivative of the Λ-type baryon mass function Σ_Λ, i.e. $\Sigma_\Lambda^\prime = \partial\,\Sigma_\Lambda/\partial \not p$, at $\not p = m_\Lambda$. The compositeness condition is the central equation of our covariant quark model. The physical meaning, the implications and corollaries of the compositeness condition have been discussed in some detail in our previous papers (see e.g. [44]).

The calculation of the Λ-type mass function (Fig.2) and the electromagnetic vertex (Fig.3) proceed in the same way as shown in the nucleon case in Ref. [45]. The matrix elements in momentum space read

$$\Sigma_\Lambda(p) = 6 g_\Lambda^2 \Big\langle\Big\langle \bar\Phi_\Lambda^2(-z_0) S_Q(k_1+w_1 p) {\rm tr}\left[S_u(k_2-w_2p)\gamma^5 S_d(k_2-k_1+w_3p)\gamma^5\right]\Big\rangle\Big\rangle\,, \tag{39}$$

where we use the same shorthand notation $<< ... >>$ for the double loop-momentum integration. The variable z_0 is defined as

$$z_0 = \tfrac{1}{2}(k_1-k_2)^2 + \tfrac{1}{6}(k_1+k_2)^2\,. \tag{40}$$

The various contributions to the electromagnetic vertex are given by

$$\begin{aligned}
\Lambda^\mu_{\Lambda\,Q}(p,p^\prime) &= 6\,e_Q\,g_\Lambda^2 \Big\langle\Big\langle \bar\Phi_\Lambda(-z_0)\bar\Phi_\Lambda\Big(-\tfrac{1}{2}(k_1-k_2+w_3q)^2 - \tfrac{1}{6}(k_1+k_2+(2w_2+w_3)q)^2\Big)\\
&\times\; S_Q(k_1+w_1p^\prime)\gamma^\mu S_Q(k_1+w_1p^\prime+q){\rm tr}\left[S_u(k_2-w_2p^\prime)\gamma^5 S_d(k_2-k_1+w_3p^\prime)\gamma^5\right]\Big\rangle\Big\rangle\,,\\
\Lambda^\mu_{\Lambda\,u}(p,p^\prime) &= -\,6\,e_u\,g_\Lambda^2 \Big\langle\Big\langle \bar\Phi_\Lambda(-z_0)\bar\Phi_\Lambda\Big(-\tfrac{1}{2}(k_1-k_2+w_3q)^2 - \tfrac{1}{6}(k_1+k_2-(2w_1+w_3)q)^2\Big)\\
&\times\; S_Q(k_1+w_1p^\prime){\rm tr}\left[S_u(k_2-w_2p^\prime-q)\gamma^\mu S_u(k_2-w_2p^\prime)\gamma^5 S_d(k_2-k_1+w_3p^\prime)\gamma^5\right]\Big\rangle\Big\rangle\,,\\
\Lambda^\mu_{\Lambda\,d}(p,p^\prime) &= 6\,e_d\,g_\Lambda^2 \Big\langle\Big\langle \bar\Phi_\Lambda(-z_0)\bar\Phi_\Lambda\Big(-\tfrac{1}{2}(k_1-k_2-(w_1+w_2)q)^2 - \tfrac{1}{6}(k_1+k_2-(w_1-w_2)q)^2\Big)\\
&\times\; S_Q(k_1+w_1p^\prime){\rm tr}\left[S_u(k_2-w_2p^\prime)\gamma^5 S_d(k_2-k_1+w_3p^\prime)\gamma^\mu S_d(k_2-k_1+w_3p^\prime+q)\gamma^5\right]\Big\rangle\Big\rangle\,,\\
\Lambda^\mu_{\Lambda\,(a)}(p,p^\prime) &= 6\,g_\Lambda^2 \Big\langle\Big\langle \bar\Phi_\Lambda(-z_0)\tilde E^\mu_\Lambda(k_1+w_1p^\prime,-k_2+w_2p^\prime,k_2-k_1+w_3p^\prime;q)\\
&\times\; S_Q(k_1+w_1p^\prime){\rm tr}\left[S_u(k_2-w_2p^\prime)\gamma^5 S_d(k_2-k_1+w_3p^\prime)\gamma^5\right]\Big\rangle\Big\rangle\,,\\
\Lambda^\mu_{\Lambda\,(b)}(p,p^\prime) &= 6\,g_\Lambda^2 \langle\langle \bar\Phi_\Lambda(-z_0)\tilde E^\mu_\Lambda(k_1+w_1p,-k_2+w_2p,k_2-k_1+w_3p;-q)\\
&\times\; S_Q(k_1+w_1p){\rm tr}\left[S_u(k_2-w_2p)\gamma^5 S_d(k_2-k_1+w_3p)\gamma^5\right]\Big\rangle\Big\rangle\,.
\end{aligned} \tag{41}$$

The free quark propagator in momentum space is given by

$$S_f(k) = \frac{1}{m_f - \not k} \tag{42}$$

where $f = u,d,s,c,b$ denotes the flavor of the freely propagating quark. We restrict ourselves to isospin invariance $m_u = m_d$. The function $\tilde E^\mu_\Lambda(r_1,r_2.r_3;r)$ is defined as

$$\widetilde E^\alpha_\Lambda(p_1,p_2,p_3;r) = \sum_{i=1}^3 e_{q_i}\int\limits_0^1 d\tau\Big\{-w_{i1}(w_{i1}r^\alpha + 2q_1^\alpha)\bar\Phi_\Lambda^\prime(-z_1) - w_{i2}(w_{i2}r^\alpha + 2q_2^\alpha)\bar\Phi_\Lambda^\prime(-z_2)\Big\}\,. \tag{43}$$

The variables $q_1 = \sum_{i=1}^3 w_{i1} r_i$ and $q_2 = \sum_{i=1}^3 w_{i2} r_i$ in $\tilde{E}^\mu_\Lambda(r_1, r_2.r_3; r)$ can be seen to be related to the loop momenta by

$$q_1 = \frac{1}{\sqrt{2}}(k_1 - k_2)\,, \qquad q_2 = -\,\frac{1}{\sqrt{6}}(k_1 + k_2) \tag{44}$$

for both bubble diagrams. By using Eq. (44) one finds the $q = 0$ relations

$$\begin{aligned}
\Lambda^\mu_{\Lambda\,(a)}(p,p) + \Lambda^\mu_{\Lambda\,(b)}(p,p) &= -\,8\,g_\Lambda^2 \Big\langle\Big\langle (Q_1 k_1^\mu + Q_2 k_2^\mu)\bar{\Phi}'_\Lambda(-z_0)\bar{\Phi}_\Lambda(-z_0) \\
&\times\; S_Q(k_1 + w_1 p)\mathrm{tr}\left[S_u(k_2 - w_2 p)\gamma^5 S_d(k_2 - k_1 + w_3 p)\gamma^5\right] \Big\rangle\Big\rangle\,,
\end{aligned}$$

$$\begin{aligned}
Q_1 &= e_1(w_2 + 2w_3) - e_2(w_1 - w_3) - e_3(2w_1 + w_2)\,, \\
Q_2 &= e_1(w_2 - w_3) - e_2(w_1 + 2w_3) + e_3(w_1 + 2w_2)\,,
\end{aligned} \tag{45}$$

where the subscripts on the charges e_i refer to the flavors of the three quarks: "$i = 1$" $\to$ "s, c, b", "$i = 2$" $\to$ "u" and "$i = 3$" $\to$ "d". Next we will use an integration-by-parts identity to write

$$\Big\langle\Big\langle \frac{\partial}{\partial k_i^\mu}\Big\{\bar{\Phi}^2_\Lambda(-z_0) S_Q(k_1 + w_1 p)\mathrm{tr}\left[S_u(k_2 - w_2 p)\gamma^5 S_d(k_2 - k_1 + w_3 p)\gamma^5\right]\Big\}\Big\rangle\Big\rangle \equiv 0\,, \qquad (i = 1, 2)\,. \tag{46}$$

One finds

$$\begin{aligned}
\Big\langle\Big\langle k_1^\mu\, A_0 \Big\rangle\Big\rangle &= \frac{1}{4}\Big\langle\Big\langle (2\,A_1^\mu + A_2^\mu - A_3^\mu)\Big\rangle\Big\rangle\,, \\
\Big\langle\Big\langle k_2^\mu\, A_0 \Big\rangle\Big\rangle &= \frac{1}{4}\Big\langle\Big\langle (A_1^\mu + 2\,A_2^\mu + A_3^\mu)\Big\rangle\Big\rangle\,,
\end{aligned} \tag{47}$$

where

$$\begin{aligned}
A_0 &= \bar{\Phi}'_\Lambda(-z_0)\,\bar{\Phi}_\Lambda(-z_0) S_Q(k_1 + w_1 p)\mathrm{tr}\left[S_u(k_2 - w_2 p)\gamma^5 S_d(k_2 - k_1 + w_3 p)\gamma^5\right]\,, \\
A_1^\mu &= \bar{\Phi}^2_\Lambda(-z_0) S_Q(k_1 + w_1 p)\gamma^\mu S_Q(k_1 + w_1 p)\mathrm{tr}\left[S_u(k_2 - w_2 p)\gamma^5 S_d(k_2 - k_1 + w_3 p)\gamma^5\right] \\
A_2^\mu &= \bar{\Phi}^2_\Lambda(-z_0) S_Q(k_1 + w_1 p)\mathrm{tr}\left[S_u(k_2 - w_2 p)\gamma^\mu S_u(k_2 - w_2 p)\gamma^5 S_d(k_2 - k_1 + w_3 p)\gamma^5\right]\,, \\
A_3^\mu &= \bar{\Phi}^2_\Lambda(-z_0) S_Q(k_1 + w_1 p)\mathrm{tr}\left[S_u(k_2 - w_2 p)\gamma^5 S_d(k_2 - k_1 + w_3 p)\gamma^\mu S_d(k_2 - k_1 + w_3 p)\gamma^5\right]\,.
\end{aligned} \tag{48}$$

Using these identities and collecting all pieces together, one obtains

$$\Lambda^\mu_\Lambda(p,p) = (e_Q + e_u + e_d)\,\frac{\partial \Sigma_\Lambda(p)}{\partial p^\mu}\,, \qquad \not{p} = m_\Lambda\,. \tag{49}$$

As was discussed above, this Ward identity allows one to use the compositeness condition $Z_\Lambda = 0$ written in the form

$$\Lambda^\mu_\Lambda(p,p) = \gamma^\mu\,, \qquad \not{p} = m_\Lambda\,, \tag{50}$$

where we take $e_Q = e_c$ for the present discussion. Again we have checked analytically that, on the Λ-type baryon mass shell, the triangle diagrams are gauge invariant by themselves and the non-gauge invariant parts coming from the bubble diagrams Fig.3(c) and 3(d) cancel each other. The standard definition of the electromagnetic form factors is

$$\Lambda^\mu_\Lambda(p,p') = \gamma_\mu F_1(q^2) - \frac{i\sigma^{\mu q}}{2m_\Lambda} F_2(q^2)\,, \tag{51}$$

where $\sigma^{\mu q} = \frac{i}{2}(\gamma^\mu\gamma^\nu - \gamma^\nu\gamma^\mu)q_\nu$. The magnetic moment of the Λ-type baryon is defined by

$$\mu_\Lambda \;=\; (\,F_1(0) + F_2(0)\,)\;\frac{e}{2m_\Lambda}\,. \tag{52}$$

In terms of the nuclear magneton (n.m.) $\frac{e}{2m_p}$ the Λ–hyperon magnetic moment is given by

$$\mu_\Lambda = \;(\,F_1(0) + F_2(0)\,)\;\frac{m_p}{m_\Lambda} \tag{53}$$

where m_p is the proton mass.

The magnetic moment has been measured for the Λ_s only and is given by [52]

$$\mu_{\Lambda_s} = -\,0.613 \pm 0.004\,. \tag{54}$$

Since we want to fit the size parameters Λ_{Λ_s}, Λ_{Λ_c} and Λ_{Λ_b} also to semileptonic $b \to c$ and $c \to s$ charged current transitions we need to briefly set up the formalism for the description of these transitions, i.e. for the transitions

$$M(\Lambda_{Q[ud]} \to \Lambda_{Q'[ud]} \ell^- \bar\nu_\ell) = \frac{G_F}{\sqrt{2}}\, V_{QQ'}\, \langle \Lambda_{Q'[ud]}\,|\,\bar Q'\, O^\mu\, Q\,|\,\Lambda_{Q[ud]}\rangle\; (\ell^-\, O_\mu\, \bar\nu_\ell)\,, \tag{55}$$

where $O^\mu = \gamma^\mu(1-\gamma_5)$. These processes are described in our model by the triangle diagram shown in Fig.4. The hadronic matrix element in (55) is expanded in terms of the dimensionless form factors f_i^J ($i=1,2,3$ and $J=V,A$), viz.

$$\begin{aligned}
\langle \Lambda_{Q'[ud]}\,|\,\bar Q'\,\gamma^\mu\, Q\,|\Lambda_{Q[ud]}\rangle \;&=\; \bar u_2(p_2)\Big[f_1^V(q^2)\gamma^\mu - f_2^V(q^2) i\sigma^{\mu q}/M_1 + f_3^V(q^2) q^\mu/M_1\Big] u_1(p_1)\,,\\
\langle \Lambda_{Q'[ud]}\,|\,\bar Q'\,\gamma^\mu\,\gamma^5 Q\,|\Lambda_{Q[ud]}\rangle \;&=\; \bar u_2(p_2)\Big[f_1^A(q^2)\gamma^\mu - f_2^A(q^2) i\sigma^{\mu q}/M_1 + f_3^A(q^2) q^\mu/M_1\Big]\gamma^5 u_1(p_1)\,.
\end{aligned} \tag{56}$$

The calculation of the form factors in our approach is automated by the use of FORM [58] and FORTRAN packages written for this purpose. To be able to compare with our earlier calculations which did not contain confinement the packages exist for the confined and the unconfined versions of the covariant quark model.

The results of our numerical calculations are well represented by the double–pole parametrization

$$f(s) = \frac{f(0)}{1 - as + bs^2}\,, \tag{57}$$

where $s = q^2/M^2_{\Lambda_i}$ and M_{Λ_i} is the mass of the initial baryon. Using such a parametrization facilitates further integrations. The values of $f(0)$, a and b are listed in Tables I-III. We plot the form factors in the full kinematical regions ($0 \le s \le s_{\max}$) in Figs. 5 ($c \to s$) and 6 ($b \to c$): solid and dotted lines correspond to approximated and exact results, respectively. The agreement between the approximate and numerically calculated form factors is excellent except for the form factors $A_2(s)$ and $T_{A1}(s)$ for which the agreement is not so good. This is due to the steep ascent of A_2 and descent of T_{A1} at the high end of the q^2 spectrum. A better fit would require the addition of a linear s term in the numerator of Eq. (57) for these two form factors.

As in the case of the rare meson decays $B \to K(K^*)\bar\ell\ell$ and $B_c \to D(D^*)\bar\ell\ell$ treated in Ref. [48] all physical observables (the rate $\Gamma(\Lambda_{Q[ud]} \to \Lambda_{Q'[ud]} + \ell^-\bar\nu_\ell)$ and asymmetry parameter α etc.) are conveniently written down in terms of helicity amplitudes H_{λ_2,λ_j}. Note that the corresponding helicity amplitudes do not carry any superscripts as they are needed in the description of the corresponding rare decays. The relations of these helicity amplitudes to the invariant form factors f_i^J is given in Appendix C. The rate for the charged current transitions can be written as

$$\Gamma(\Lambda_{Q[ud]} \to \Lambda_{Q'[ud]} + \ell^-\bar\nu_\ell) \;=\; \frac{G_F^2 |V_{QQ'}|^2}{192\pi^3 M_1^2} \int\limits_{m_\ell^2}^{(M_1-M_2)^2} \frac{dq^2}{q^2}\,(q^2 - m_\ell^2)^2\,|\mathbf{p_2}|\;\mathcal{H}\,. \tag{58}$$

For the asymmetry parameter α in these decays (see Ref. [34] for the definition of the asymmetry parameter) one obtains

$$\alpha \;=\; \frac{\int\limits_{m_\ell^2}^{(M_1-M_2)^2} \frac{dq^2}{q^2}\,(q^2-m_\ell^2)^2\,|\mathbf{p_2}|\;\mathcal{G}}{\int\limits_{m_\ell^2}^{(M_1-M_2)^2} \frac{dq^2}{q^2}\,(q^2-m_\ell^2)^2\,|\mathbf{p_2}|\;\mathcal{H}}\,, \tag{59}$$

where

$$\begin{aligned}
\mathcal{H} \;&=\; H_U + H_L + \frac{m_\ell^2}{2q^2}\Big(3H_S + H_U + H_L\Big)\,,\\
\mathcal{G} \;&=\; H_P + H_{L_P} + \frac{m_\ell^2}{2q^2}\Big(3H_{S_P} + H_P + H_{L_P}\Big)\,,
\end{aligned} \tag{60}$$

and the H_X are the following combinations of the helicity amplitudes:

$$
\begin{aligned}
H_U &= |H_{\frac{1}{2}1}|^2 + |H_{-\frac{1}{2}-1}|^2 \,, \\
H_L &= |H_{\frac{1}{2}0}|^2 + |H_{-\frac{1}{2}0}|^2 \,, \\
H_P &= |H_{\frac{1}{2}1}|^2 - |H_{-\frac{1}{2}-1}|^2 \,, \\
H_{L_P} &= |H_{\frac{1}{2}0}|^2 - |H_{-\frac{1}{2}0}|^2 \,, \\
H_S &= |H_{\frac{1}{2}t}|^2 + |H_{-\frac{1}{2}t}|^2 \,, \\
H_{S_P} &= |H_{\frac{1}{2}t}|^2 - |H_{-\frac{1}{2}t}|^2 \,.
\end{aligned}
\tag{61}
$$

We determine the set of size parameters Λ_{Λ_s}, Λ_{Λ_c} and Λ_{Λ_b} by fitting data on the magnetic moment of the Λ-hyperon (54) and the nominal branching ratios of the semileptonic decays $\Lambda_c \to \Lambda\ell^+\nu_\ell$ and $\Lambda_b \to \Lambda_c\ell^-\bar{\nu}_\ell$ by a one-parameter fit to these values. Using the results of Table II for the $\Lambda_b \to \Lambda_c$ case one finds the zero recoil values $f_1^V = 0.87$ and $f_1^A = 0.86$. These form factor values are somewhat lower than the values $f_1^V = f_1^A = 1$ predicted by HQET. This can be interpreted as an indication that the nominal value for the $\Lambda_b \to \Lambda_c\ell^-\bar{\nu}_\ell$ branching ratio listed in the Particle Data Group [52] and used by us in our fit is underestimated. With the choice of dimensional parameters $\Lambda_{\Lambda_s} = 0.490$ GeV, $\Lambda_{\Lambda_c} = 0.864$ GeV and $\Lambda_{\Lambda_b} = 0.569$ GeV we get a reasonable agreement with current data on exclusive Cabibbo-allowed decays of Λ_c and Λ_b (see Tables IV and V). For the magnetic moments we get the following results:

$$
\mu_{\Lambda_s} = -0.73\,, \quad \mu_{\Lambda_c} = 0.39\,, \quad \mu_{\Lambda_b} = -0.06\,,
\tag{62}
$$

which compares well with data for the μ_{Λ_s} and theoretical estimates for the μ_{Λ_c} and μ_{Λ_b} (see the detailed discussion in Ref. [40]). In particular, our present results for the magnetic moments of heavy Λ-hyperons are very close to our predictions done before in the model without taking account of the mechanism of quark confinement: $\mu_{\Lambda_c} = 0.42$ and $\mu_{\Lambda_b} = -0.06$ [40]. Note, the other model parameters m_q and λ are taken from the fit done in the Ref. [46]:

m_u	m_s	m_c	m_b	λ	
0.235	0.424	2.16	5.09	0.181	GeV

(63)

IV. THE RARE BARYON DECAYS $\Lambda_b \to \Lambda + \ell^+\ell^-$ AND $\Lambda_b \to \Lambda + \gamma$

The effective Hamiltonian [59] leads to the quark decay amplitudes $b \to sl^+l^-$ and $b \to s\gamma$:

$$
\begin{aligned}
M(b \to s\ell^+\ell^-) &= \frac{G_F}{\sqrt{2}}\frac{\alpha\lambda_t}{2\pi}\Big\{C_9^{\rm eff}\,(\bar{s}O^\mu b)\,\big(\bar{\ell}\gamma_\mu\ell\big) + C_{10}\,(\bar{s}O^\mu b)\,\big(\bar{\ell}\gamma_\mu\gamma_5\ell\big) \\
&- \frac{2}{q^2}\,C_7^{\rm eff}\,\big[m_b\,\big(\bar{s}\,i\sigma^{\mu q}\,(1+\gamma^5)\,b\big) + m_s\,\big(\bar{s}\,i\sigma^{\mu q}\,(1-\gamma^5)\,b\big)\big]\,\big(\bar{\ell}\gamma_\mu\ell\big)\Big\}\,.
\end{aligned}
\tag{64}
$$

and

$$
M(b \to s\gamma) = -\frac{G_F}{\sqrt{2}}\frac{e\lambda_t}{4\pi^2}\,C_7^{\rm eff}\,\big[m_b\,\big(\bar{s}\,i\sigma^{\mu q}\,(1+\gamma^5)\,b\big) + m_s\,\big(\bar{s}\,i\sigma^{\mu q}\,(1-\gamma^5)\,b\big)\big]\,\epsilon_\mu\,,
\tag{65}
$$

where $\sigma^{\mu q} = \frac{i}{2}(\gamma^\mu\gamma^\nu - \gamma^\nu\gamma^\mu)q_\nu$, $O^\mu = \gamma^\mu(1-\gamma^5)$ and $\lambda_t \equiv V_{ts}^\dagger V_{tb}$. The Wilson coefficient $C_9^{\rm eff}$ effectively takes into account, first, the contributions from the four-quark operators $Q_i (i = 1, \cdots, 6)$ and, second, the nonperturbative effects (long–distance contributions) coming from the $c\bar{c}$-resonance contributions what are, as usual, parametrized by a Breit-Wigner ansatz [60] (see details in Appendix D).

The Feynman diagrams contributing to the exclusive transitions $\Lambda_b \to \Lambda\bar{\ell}\ell$ and $\Lambda_b \to \Lambda\gamma$ are shown in Fig.6. The corresponding matrix elements of the exclusive transitions $\Lambda_b \to \Lambda\bar{\ell}\ell$ and $\Lambda_b \to \Lambda\gamma$ are defined by

$$
\begin{aligned}
M(\Lambda_b \to \Lambda\bar{\ell}\ell) &= \frac{G_F}{\sqrt{2}}\frac{\alpha\lambda_t}{2\,\pi}\Big\{C_9^{\rm eff}\,\langle\Lambda\,|\,\bar{s}\,O^\mu\,b\,|\,\Lambda_b\rangle\,\bar{\ell}\gamma_\mu\ell \\
&+ C_{10}\,\langle\Lambda\,|\,\bar{s}\,O^\mu\,b\,|\,\Lambda_b\rangle\,\bar{\ell}\gamma_\mu\gamma_5\ell \\
&- \frac{2m_b}{q^2}\,C_7^{\rm eff}\,\langle\Lambda\,|\,\bar{s}\,i\sigma^{\mu q}\,(1+\gamma^5)\,b\,|\,\Lambda_b\rangle\,\bar{\ell}\gamma_\mu\ell\Big\}
\end{aligned}
\tag{66}
$$

and

$$M(\Lambda_b \to \Lambda\gamma) = -\frac{G_F}{\sqrt{2}}\frac{e\lambda_t}{4\,\pi^2}\, m_b\, C_7^{\rm eff}\, \langle \Lambda \,|\, \bar{s}\, i\sigma^{\mu q}\, (1+\gamma^5)\; b \,|\, \Lambda_b\rangle\, \epsilon_\mu\,. \tag{67}$$

The hadronic matrix elements in (66) and (67) are expanded in terms of dimensionless form factors f_i^J ($i=1,2,3$ and $J=V,A,TV,TA$), viz.

$$\begin{aligned}
\langle B_2\,|\,\bar{s}\,\gamma^\mu\, b\,|B_1\rangle &= \bar{u}_2(p_2)\Big[f_1^V(q^2)\gamma^\mu - f_2^V(q^2)i\sigma^{\mu q}/M_1 + f_3^V(q^2)q^\mu/M_1\Big]u_1(p_1)\,,\\
\langle B_2\,|\,\bar{s}\,\gamma^\mu\gamma^5\, b\,|B_1\rangle &= \bar{u}_2(p_2)\Big[f_1^A(q^2)\gamma^\mu - f_2^A(q^2)i\sigma^{\mu q}/M_1 + f_3^A(q^2)q^\mu/M_1\Big]\gamma^5 u_1(p_1)\,,\\
\langle B_2\,|\,\bar{s}\, i\sigma^{\mu q}/M_1\, b\,|B_1\rangle &= \bar{u}_2(p_2)\Big[f_1^{TV}(q^2)(\gamma^\mu q^2 - q^\mu\,\not{q})/M_1^2 - f_2^{TV}(q^2)i\sigma^{\mu q}/M_1\Big]u_1(p_1)\,,\\
\langle B_2\,|\,\bar{s}\, i\sigma^{\mu q}\gamma^5/M_1\, b\,|B_1\rangle &= \bar{u}_2(p_2)\Big[f_1^{TA}(q^2)(\gamma^\mu q^2 - q^\mu\,\not{q})/M_1^2 - f_2^{TA}(q^2)i\sigma^{\mu q}/M_1\Big]\gamma^5 u_1(p_1)\,.
\end{aligned} \tag{68}$$

One can see that, in comparison with the Cabibbo-allowed $b\to c$ and $c\to s$ transitions, one has four more form factors $f_{1,2}^{TV,TA}$. As was mentioned before, the numerical results for the invariant form factors are well represented by the double–pole parametrization (57). The values of $f(0)$, a and b for the approximated form factors describing the $b\to s$ flavor transitions are listed in Table III. The plots of the form factors in the full kinematical regions ($0\le s\le s_{\rm max}$) are shown in Fig. 7: the solid and dotted lines correspond to approximated and exact results, respectively. One can see that both curves are in close agreement with each other. There is only a small disagreement for the suppressed form factors f_2^A and f_2^{TA}.

Note, that a form factor approximation similar to the form (57) was successfully used by us in Ref. [48] in the analysis of rare decays of bottom mesons. The relations of the helicity amplitudes and invariant form factors are given in Appendix C.

Similar to Eq. (24) the angular decay distribution for the cascade decay $\Lambda_b\to\Lambda(\to p\pi^-)\gamma$ can be written as

$$\frac{d\Gamma(\Lambda_b\to\Lambda(\to p\pi^-)\gamma)}{d\cos\theta_B} = {\rm Br}(\Lambda\to p\pi^-)\,\frac{1}{2}\,\Gamma(\Lambda_b\to\Lambda\gamma)(1+\alpha_B P_z^\Lambda\cos\theta_B)\,, \tag{69}$$

where α_B is the asymmetry parameter in the decay $\Lambda\to p+\pi^-$ for which we take the experimental value $\alpha_B = 0.642\pm 0.013$ [52]. The $\Lambda_b\to\Lambda\gamma$ decay rate is calculated according to

$$\begin{aligned}
\Gamma(\Lambda_b\to\Lambda\gamma) &= \frac{\alpha}{2}\left(\frac{G_F\,M_1^2\,|\lambda_t|}{4\pi^2\sqrt{2}}\right)^2\frac{|\mathbf{p_2}|}{2M_1^2}\,\Big[|H^V_{\frac12 1}|^2 + |H^V_{-\frac12 -1}|^2 + |H^A_{\frac12 1}|^2 + |H^A_{-\frac12 -1}|^2\Big]\\
&= \frac{\alpha}{2}\left(\frac{G_F m_b\,|\lambda_t|\,C_7^{\rm eff}}{4\pi^2\sqrt{2}}\right)^2\frac{(M_1^2-M_2^2)^3}{M_1^3}\,\left[\Big(f_2^{TV}(0)\Big)^2 + \Big(f_2^{TA}(0)\Big)^2\right].
\end{aligned} \tag{70}$$

As before the expressions of helicity amplitudes in terms of invariant form factors are given in Appendix C. The z–component of the polarization of the Λ appearing in Eq. (69) is given by

$$\tilde{P}_z^\Lambda = \frac{\tilde{W}_{\frac12\frac12} - \tilde{W}_{-\frac12-\frac12}}{\tilde{W}_{\frac12\frac12} + \tilde{W}_{-\frac12-\frac12}} \tag{71}$$

where

$$\tilde{W}_{\lambda_\Lambda\lambda_\Lambda} \propto H_{\lambda_\Lambda,\lambda_j=2\lambda_\Lambda} H^\dagger_{\lambda_\Lambda,\lambda_j=2\lambda_\Lambda}\,. \tag{72}$$

We have used a tilde notation in $\tilde{P}_z^\Lambda$ and $\tilde{W}_{\lambda_\Lambda\lambda_\Lambda}$ in order to distinguish these quantities from the corresponding quantities in the dilepton modes. One has,

$$\tilde{P}_z^\Lambda = -2\frac{f_2^{TV}(0)f_2^{TA}(0)}{(f_2^{TV}(0))^2 + (f_2^{TA}(0))^2}\,. \tag{73}$$

Note, that $f_2^{TV}(0)\equiv f_2^{TA}(0)$ (see proof in Appendix E), which is in agreement with statement of Ref. [61]. Therefore, $\tilde{P}_z^\Lambda\equiv -1$ and finally

$$\frac{1}{\Gamma_{\rm tot}}\,\frac{d\Gamma(\Lambda_b\to\Lambda(\to p\pi^-)\gamma)}{d\cos\theta_B} = {\rm Br}(\Lambda\to p\pi^-)\,\frac{1}{2}\,{\rm Br}(\Lambda_b\to\Lambda\gamma)(1-\alpha_B\cos\theta_B)\,. \tag{74}$$

V. NUMERICAL RESULTS

In this section we present a detailed numerical analysis of the rare decays $\Lambda_b \to \Lambda\ell^+\ell^-$ and $\Lambda_b \to \Lambda\gamma$. In Figs. 8-26 we present two-dimensional and three-dimensional polar angle and polarization distributions. Our predictions for differential rates are shown in the two-dimensional plots Figs. 8-10, lepton-side and hadron-side forward-backward asymmetries are displayed in Figs. 14-16 and in Figs. 23-25, respectively. In all the three cases we plot two respective results what are labelled by "LD" (including long-distance contributions) and "NLD" (no long-distance contributions). In Figs. 11-13 we provide three-dimensional plots of the s-dependence of the lepton-side polar angle decay distributions for each of the e, μ and τ-cases. In Figs. 17-19 we do the same for the hadron-side decay distribution. One clearly sees the long-distance contributions of the charmonium resonances. In Figs. 20-22 we show plots of of the $\cos\theta$ and s dependence of the longitudinal polarization P_z^Λ of the daughter baryon Λ, again for the e, μ and τ-cases. The polarization is large and negative in all cases. Finally, in Fig. 26 we show the (hadron-side) polar angle distribution of the radiative decay $\Lambda_b \to \Lambda(\to p\pi^-)\gamma$. As expected from Eq. (74) and from the discussion in Sec. IV the $\cos\theta_B$ dependence is given by a straight-line plot with a slope proportional to the asymmetry parameter α_B.

In Table VI we present our results for the branching ratios of the rare dileptonic decay $\Lambda_b \to \Lambda\ell^+\ell^-$. The results without long-distance effects are shown in brackets. Our predictions for the radiative decay $\Lambda_b \to \Lambda\gamma$ are shown in Table VII. Here we also present the results of other approaches using the compilation of Ref. [18]. The results for the integrated lepton–side and hadron–side forward–backward asymmetries are shown in Tables VIII.

In our calculations we do not include the regions around the two charmonium resonances $R_{c\bar{c}} = J/\psi, \Psi(2S)$. We exclude the regions $M_{J/\Psi} - 0.20$ GeV to $M_{J/\Psi} + 0.04$ GeV and $M_{\Psi(2S)} - 0.10$ GeV to $M_{\Psi(2S)} + 0.02$ GeV. As stressed in Ref. [7] these regions are experimentally vetoed, because the rates of nonleptonic decays $\Lambda_b \to \Lambda + R_{c\bar{c}}$, followed by the dileptonic decays of the charmonium, are much larger than rates of the $b \to s$-induced rare decays $\Lambda_b \to \Lambda\ell^+\ell^-$. Vetoing the regions near the charmonium resonances leads to physically acceptable results — the predictions with and without the inclusion of long–distance effects are comparable with each other. Otherwise (without such a vetoing) the results with long–distance effects are dramatically enhanced (as shown in different theoretical calculations, see also results in Table VI).

VI. SUMMARY AND CONCLUSIONS

i) We have used the helicity formalism to express a number of observables in the rare baryon decay $\Lambda_b \to \Lambda(\to p\pi^-)\,\ell^+\ell^-$ in terms of a basic set of hadronic helicity structure functions. In the helicity method one provides complete information on the spin density matrix of each particle in the cascade decay chain which can be conveniently read out by considering angular decay distributions in the rest frame of that particular particle. We hope that we have demonstrated the advantages of the helicity method over a traditional covariant calculation. Every conceivable observable can be written in terms of bilinear forms of the basic hadronic helicity amplitudes calculated in this paper while a covariant evaluation requires an *ab initio* calculation for every new observable. We have provided some examples of such observables in this paper.

ii) There is a multitude of observables to be explored experimentally and theoretically. These include the polarization of the decaying baryon and single–lepton and double–lepton polarization asymmetries what have not been discussed in this paper. The advantage of the helicity method is that it is straightforward to define any of the observables of the problem and to express them in terms of bilinear forms of the hadronic helicity matrix elements defined and calculated in this paper. There is no need to restart a covariant calculation for every new spin observable. We mention that it is well–known that hadronically produced hyperons are found to be partially polarized perpendicular to the production plane. Similar polarization effects are expected to occur for hadronically produced Λ_b's. Also Λ_b's from $Z \to \Lambda_b\bar{\Lambda}_b$ are expected to be highly polarized. It would be important to take into account such polarization effects in the angular decay distribution of the Λ_b.

iii) We have provided results with and without taking the so–called long distance effects into account, for which the long distance effects are calculated by the contributions of the J/Ψ and $\Psi(2S)$ resonances.

iv) We have described from a unified point of view exclusive Cabibbo-allowed semileptonic decays $\Lambda_b \to \Lambda_c\ell^-\bar{\nu}_\ell$, $\Lambda_c \to \Lambda\ell^+\nu_\ell$ and rare decays $\Lambda_b \to \Lambda\ell^+\ell^-$, $\Lambda_b \to \Lambda\gamma$ with the use of only three model parameters: the size parameters Λ_{Λ_s}, Λ_{Λ_c} and Λ_{Λ_b} defining the distribution of quarks in the Λ, Λ_c and Λ_b baryons.

v) The helicity formulas introduced in this paper can be used as input in a MC event generator patterned after the existing event generator for $\Xi^0(\uparrow) \to \Sigma^+(\to p\pi^0)\ell^-\bar{\nu}_\ell\ \ell = (e, \mu)$ which is described and put to use in [47] and which has been used by the NA48 Collaboration to analyze its data on the above decay [62]. Such a MC event generator would require a viable parametrization of the hadronic transition helicity amplitudes for the whole range of q^2 which we provide in this paper.

vi) In a future work, we plan to discuss further rare baryonic ($b \to s$) and ($b \to d$) decays such as $\Omega_b^- \to \Omega^- \ell^+\ell^-$, $\Xi_b^- \to \Sigma^- \ell^+\ell^-$, etc., and $\Lambda_b \to n\,\ell^+\ell^-$. We shall then also compare our form factor results with the results of other model calculations.

vii) In this future work we shall also discuss the full three–fold joint angular decay distribution including a treatment of Λ_b polarization effects as well as single lepton polarization effects.

Acknowledgments

This work was supported by the DFG under Contract No. LY 114/2-1, by Federal Targeted Program "Scientific and scientific-pedagogical personnel of innovative Russia" Contract No.02.740.11.0238. The work is done partially under the project 2.3684.2011 of Tomsk State University. M.A.I. acknowledges the support of the Forschungszentrum of the Johannes Gutenberg–Universität Mainz "Elementarkräfte und Mathematische Grundlagen (EMG)" and the Heisenberg-Landau Grant. M.A.I. and V.E.L. would like to thank Dipartimento di Fisica, Università di Napoli Federico II and Istituto Nazionale di Fisica Nucleare, Sezione di Napoli for warm hospitality.

Appendix A: Joint four-fold angular decay distribution for the decay of an unpolarized Λ_b

We write out the three-fold angular decay distribution Eq. (1) where we collect together terms with the threshold behavior v^0, v^1 and v^2. Including the q^2 dependence one obtains a four-fold joint angular decay distribution for the decay of an unpolarized Λ_b. One has

$$W(\theta,\theta_B,\chi) \propto \frac{32\,q^2}{9}\Big(|h^B_{\frac12 0}|^2 + |h^B_{-\frac12 0}|^2\Big)\Big(A\,v^2 + B\,v + C\,\frac{2m_\ell^2}{q^2}\Big)\,, \tag{A1}$$

where the coefficients A,B and C are given by

$$\begin{aligned}
A &= \frac{9}{64}\,(1+\cos^2\theta)\,\big(U^{11}+U^{22}\big) + \frac{9}{32}\,\sin^2\theta\,\big(L^{11}+L^{22}\big)\\
&+ \frac{9}{32}\,\alpha_B\,\cos\theta_B\Big[\sin^2\theta\,\big(L_P^{11}+L_P^{22}\big) + \frac12\,(1+\cos^2\theta)\,\big(P^{11}+P^{22}\big)\Big]\\
&+ \frac{9}{16\sqrt2}\,\alpha_B\,\sin 2\theta\,\sin\theta_B\Big[\cos\chi\,\big(I1_P^{11}+I1_P^{22}\big) - \sin\chi\,\big(I2_P^{11}+I2_P^{22}\big)\Big]\,,\\
B &= -\frac{9}{16}\,\cos\theta\Big[P^{12}+\alpha_B\,\cos\theta_B\,U^{12}\Big]\\
&- \frac{9}{4\sqrt2}\,\alpha_B\,\sin\theta\,\sin\theta_B\Big[\cos\chi\,I3_P^{12} - \sin\chi\,I4_P^{12}\Big]\,,\\
C &= \frac{9}{16}\,\big(U^{11}+L^{11}+S^{22}\big) + \frac{9}{16}\,\alpha_B\,\cos\theta_B\,\big(P^{11}+L_P^{11}+S_P^{22}\big)\,,
\end{aligned}$$

The bilinear expressions $H_X^{mm'}$ ($X = U, L, S, P, L_P, S_P, I1_P, I2_P, I3_P, I4_P$) are defined by

$$
\begin{aligned}
H_U^{mm'} &= \mathrm{Re}(H^m_{\frac12 1} H^{\dagger m'}_{\frac12 1}) + \mathrm{Re}(H^m_{-\frac12 -1} H^{\dagger m'}_{-\frac12 -1}) && \text{transverse unpolarized}\,,\\
H_L^{mm'} &= \mathrm{Re}(H^m_{\frac12 0} H^{\dagger m'}_{\frac12 0}) + \mathrm{Re}(H^m_{-\frac12 0} H^{\dagger m'}_{-\frac12 0}) && \text{longitudinal unpolarized}\,,\\
H_S^{mm'} &= \mathrm{Re}(H^m_{\frac12 t} H^{\dagger m'}_{\frac12 t}) + \mathrm{Re}(H^m_{-\frac12 t} H^{\dagger m'}_{-\frac12 t}) && \text{scalar unpolarized}\,,\\
H_P^{mm'} &= \mathrm{Re}(H^m_{\frac12 1} H^{\dagger m'}_{\frac12 1}) - \mathrm{Re}(H^m_{-\frac12 -1} H^{\dagger m'}_{-\frac12 -1}) && \text{transverse parity–odd polarized}\,,\\
H_{L_P}^{mm'} &= \mathrm{Re}(H^m_{1/2\,0} H^{\dagger m'}_{1/2\,0} - H^m_{-1/2\,0} H^{\dagger m'}_{-1/2\,0}) && \text{longitudinal polarized}\,,\\
H_{S_P}^{mm'} &= \mathrm{Re}(H^m_{1/2\,t} H^{\dagger m'}_{1/2\,t} - H^m_{-1/2\,t} H^{\dagger m'}_{-1/2\,t}) && \text{scalar polarized}\,,\\
H_{I1_P}^{mm'} &= \tfrac14 \mathrm{Re}(H^m_{1/2\,1} H^{\dagger m'}_{-1/2\,0} + H^m_{-1/2\,0} H^{\dagger m'}_{1/2\,1} \\
&\quad - H^m_{-1/2\,-1} H^{\dagger m'}_{1/2\,0} - H^m_{1/2\,0} H^{\dagger m'}_{-1/2\,-1}) && \text{longitudinal–transverse interference (1)}\,,\\
H_{I2_P}^{mm'} &= \tfrac14 \mathrm{Im}(H^m_{1/2\,1} H^{\dagger m'}_{-1/2\,0} - H^m_{-1/2\,0} H^{\dagger m'}_{1/2\,1} \\
&\quad + H^m_{-1/2\,-1} H^{\dagger m'}_{1/2\,0} - H^m_{1/2\,0} H^{\dagger m'}_{-1/2\,-1}) && \text{longitudinal–transverse interference (2)}\,,\\
H_{I3_P}^{mm'} &= \tfrac14 \mathrm{Re}(H^m_{1/2\,1} H^{\dagger m'}_{-1/2\,0} + H^m_{-1/2\,0} H^{\dagger m'}_{1/2\,1} \\
&\quad + H^m_{-1/2\,-1} H^{\dagger m'}_{1/2\,0} + H^m_{1/2\,0} H^{\dagger m'}_{-1/2\,-1}) && \text{longitudinal–transverse interference (3)}\,,\\
H_{I4_P}^{mm'} &= \tfrac14 \mathrm{Im}(H^m_{1/2\,1} H^{\dagger m'}_{-1/2\,0} - H^m_{-1/2\,0} H^{\dagger m'}_{1/2\,1} \\
&\quad - H^m_{-1/2\,-1} H^{\dagger m'}_{1/2\,0} + H^m_{1/2\,0} H^{\dagger m'}_{-1/2\,-1}) && \text{longitudinal–transverse interference (4)}\,.
\end{aligned}
\tag{A2}
$$

Note the three-fold joint angular decay distribution for the decay of an unpolarized Λ_b is factorized in terms of fully transverse (unpolarized and parity–odd polarized), longitudinal (upolarized and polarized), scalar (unpolarized and polarized) bilinear helicity combinations and four combinations of longitudinal-transverse interference.

Another important property of the three-fold joint angular decay distribution is its invariance w.r.t. the choice of coordinate systems. For example, using the completeness relation for the polarization vectors of the effective current one can explicitly show that the angular decay distribution Eq. (A1) is the same for two specific choices of coordinate systems: system (i) $\vec{J}_{\rm eff}$ is directed along the z-axis as in this paper and system (ii) $\vec{J}_{\rm eff}$ is antiparallel to the direction of the z-axis as used e.g. in Refs. [42, 43, 47]). In particular, only the transverse helicity amplitudes $H^m_{\pm 1/2\,\pm 1}$ change sign when going from system (i) to system (ii) while the other helicity amplitudes remain invariant. The change of sign for the transverse amplitudes $H^m_{\pm 1/2\,\pm 1}$ can be seen to be compensated by the effects of rotating the coordinate system (i) by 180° around the x-axis when going from system (i) to system (ii).

Appendix B: Interpolating currents of Λ-hyperons

When constructing interpolating baryon currents it is convenient to use Fierz transformations and corresponding identities in order to interchange the quark fields. First we specify five possible spin structures $J^{\alpha\beta,\rho\sigma} = \Gamma_1^{\alpha\beta} \otimes (C\Gamma_2)^{\rho\sigma}$ defining the Fierz transformation of the baryon currents:

$$
\begin{aligned}
P &= I \otimes C\gamma_5\,,\\
S &= \gamma_5 \otimes C\,,\\
A &= \gamma^\mu \otimes C\gamma_5\gamma_\mu\,,\\
V &= \gamma^\mu\gamma^5 \otimes C\gamma_\mu\,,\\
T &= \frac12 \sigma^{\mu\nu}\gamma^5 \otimes C\sigma_{\mu\nu}\,.
\end{aligned}
\tag{B1}
$$

The Fierz transformation of the structures $J = \{P, S, A, V, T\}$ read

$$
\begin{aligned}
P &= \frac{1}{4}\biggl(\tilde{P} + \tilde{S} + \tilde{A} + \tilde{V} + \tilde{T}\biggr), \\
S &= \frac{1}{4}\biggl(\tilde{P} + \tilde{S} - \tilde{A} - \tilde{V} + \tilde{T}\biggr), \\
A &= \tilde{P} - \tilde{S} - \frac{1}{2}\biggl(\tilde{A} - \tilde{V}\biggr), \\
V &= \tilde{P} - \tilde{S} + \frac{1}{2}\biggl(\tilde{A} - \tilde{V}\biggr), \\
T &= \frac{3}{2}(\tilde{P} + \tilde{S}) - \frac{1}{2}\tilde{T}.
\end{aligned}
\tag{B2}
$$

The symbol $\tilde{}$ is used to denote Fierz-transformed matrices according to $\tilde{J}^{\alpha\sigma,\rho\beta} = \Gamma_1^{\alpha\sigma} \otimes (C\Gamma_2)^{\rho\beta}$ where α, β, ρ and σ are Dirac indices. Using Eqs. (B2) one can derive useful identities

$$
\begin{aligned}
2(P - S) + A + V &= 2(\tilde{P} - \tilde{S}) + \tilde{A} + \tilde{V}, \\
3(P + S) + T &= 3(\tilde{P} + \tilde{S}) + \tilde{T}.
\end{aligned}
\tag{B3}
$$

Let us consider hyperons containing two light nonstrange u or d quarks and a third quark $Q = s, c$ or b, which contain antisymmetrized combination of u and d quarks over spin and flavor. There are two possible SU(N$_\mathrm{f}$)-symmetric interpolating currents of Λ-hyperons without derivatives — the so-called vector $J^V_{\Lambda_{Q[ud]}}$ and tensor $J^T_{\Lambda_{Q[ud]}}$ current:

$$
\begin{aligned}
J^V_{\Lambda_{Q[ud]}} &= \frac{1}{3}\,\epsilon^{a_1a_2a_3}\,\left(\gamma^\mu\gamma^5 d^{a_1} u^{a_2} C\gamma_\mu Q^{a_3} - \gamma^\mu\gamma^5 u^{a_1} d^{a_2} C\gamma_\mu Q^{a_3}\right), \\
J^T_{\Lambda_{Q[ud]}} &= \frac{1}{3}\,\epsilon^{a_1a_2a_3}\,\left(\sigma^{\mu\nu}\gamma^5 d^{a_1} u^{a_2} C\sigma_{\mu\nu} Q^{a_3} - \sigma^{\mu\nu}\gamma^5 u^{a_1} d^{a_2} C\sigma_{\mu\nu} Q^{a_3}\right).
\end{aligned}
\tag{B4}
$$

Using Fierz transformations one can rewrite $J^V_{\Lambda_{Q[ud]}}$ and $J^T_{\Lambda_{Q[ud]}}$ currents as a linear combination of more convenient currents — pseudoscalar $J^P_{\Lambda_{Q[ud]}}$, scalar $J^S_{\Lambda_{Q[ud]}}$ and axial $J^A_{\Lambda_{Q[ud]}}$, which manifestly contain the spin-0 $[ud]$-diquark:

$$
\begin{aligned}
J^P_{\Lambda_{Q[ud]}} &= \epsilon^{a_1a_2a_3}\, Q^{a_1}\, u^{a_2} C\gamma_5 d^{a_3}, \\
J^S_{\Lambda_{Q[ud]}} &= \epsilon^{a_1a_2a_3}\, \gamma^5\, Q^{a_1}\, u^{a_2} C d^{a_3}, \\
J^A_{\Lambda_{Q[ud]}} &= \epsilon^{a_1a_2a_3}\, \gamma^\mu\, u^{a_1}\, d^{a_2} C\gamma_5\gamma_\mu q_3^{a_3}.
\end{aligned}
\tag{B5}
$$

The result after the Fierz transformation reads:

$$
\begin{aligned}
J^V_{\Lambda_{Q[ud]}} &= \frac{2}{3} J^P_{\Lambda_{Q[ud]}} - \frac{2}{3} J^S_{\Lambda_{Q[ud]}} + \frac{1}{3} J^A_{\Lambda_{Q[ud]}}, \\
J^T_{\Lambda_{Q[ud]}} &= J^P_{\Lambda_{Q[ud]}} + J^S_{\Lambda_{Q[ud]}}.
\end{aligned}
\tag{B6}
$$

It is clear that in the nonrelativistic limit the J^V and J^T currents become degenerate and coincide with the J^P and J^A currents. Therefore, the J^P and J^A currents differ from SU(N$_\mathrm{f}$) currents up to relativistic corrections.

Appendix C: Helicity amplitudes

In Sec.II we have shown how to write out the angular distributions of the rare Λ_b decays in terms of hadron–side helicity amplitudes $H^m_{\lambda_2,\lambda_j}$, which in turn can be related to invariant form factors f_i^J (see details Refs. [42, 43, 47]). The pertinent relation is

$$
H^m_{\lambda_2,\lambda_j} = M^m_\mu(\lambda_2)\,\epsilon^{*\mu}(\lambda_j). \tag{C1}
$$

As before the labels λ_2 and λ_j denote the helicities of the daughter baryon and the effective current, corresponding to the lepton pair and the photon, respectively. We shall work in the rest frame of the parent baryon B_1 with the daughter baryon B_2 moving in the negative z-direction (see Fig.1) such that $p_1^\mu = (M_1, \mathbf{0})$, $p_2^\mu = (E_2, 0, 0, -|\mathbf{p}_2|)$ and

$q^\mu = (q_0, 0, 0, |\mathbf{p}_2|)$, where $q_0 = (M_1^2 - M_2^2 + q^2)/(2M_1)$ and $E_2 = M_1 - q_0 = (M_1^2 + M_2^2 - q^2)/(2M_1)$. Angular momentum conservation fixes the helicity λ_1 of the parent baryon according to $\lambda_1 = -\lambda_2 + \lambda_j$.

The $J = \frac{1}{2}$ baryon spinors are given by

$$\begin{aligned}
\bar{u}_2\Big(p_2, \pm\frac{1}{2}\Big) &= \sqrt{E_2 + M_2}\,\Big(\chi_\pm^\dagger, \frac{\pm|\mathbf{p}_2|}{E_2 + M_2}\chi_\pm^\dagger\Big)\,, \\
u_1\Big(p_1, \pm\frac{1}{2}\Big) &= \sqrt{2M_1}\,\begin{pmatrix} \chi_\pm \\ 0 \end{pmatrix}\,,
\end{aligned} \tag{C2}$$

where $\chi_+ = \begin{pmatrix} 1 \\ 0 \end{pmatrix}$ and $\chi_- = \begin{pmatrix} 0 \\ 1 \end{pmatrix}$ are two–component Pauli spinors.

The polarization vectors of the effective current $J_{\rm eff}$ read

$$\begin{aligned}
\epsilon^\mu(t) &= \frac{1}{\sqrt{q^2}}(\,q_0\,,\ 0\,,\ 0\,,\ |\mathbf{p_2}|\,)\,, \\
\epsilon^\mu(\pm) &= \frac{1}{\sqrt{2}}(\,0\,,\ \mp 1\,,\ -i\,,\ 0\,)\,, \\
\epsilon^\mu(0) &= \frac{1}{\sqrt{q^2}}(\,|\mathbf{p_2}|\,,\ 0\,,\ 0\,,\ q_0\,)\,.
\end{aligned} \tag{C3}$$

Using this basis one can express the components of the hadronic tensors through the invariant form factors. It is convenient to split the helicity amplitudes on vector ($H^{Vm}_{\lambda_2,\lambda_j}$) and axial–vector ($H^{Am}_{\lambda_2,\lambda_j}$) parts:

$$H^m_{\lambda_2,\lambda_j} = H^{Vm}_{\lambda_2,\lambda_j} - H^{Am}_{\lambda_2,\lambda_j}\,. \tag{C4}$$

From parity or from an explicit calculation one has

$$\begin{aligned}
H^{Vm}_{-\lambda_2,-\lambda_j} &= H^{Vm}_{\lambda_2,\lambda_j}\,, \\
H^{Am}_{-\lambda_2,-\lambda_j} &= -H^{Am}_{\lambda_2,\lambda_j}\,.
\end{aligned} \tag{C5}$$

In the case of the transitions $\Lambda_{q_1[q2q3]} \to \Lambda_{q_1'[q_2q_3]} + j_{\rm eff}$ the helicity amplitudes $H^{Vm}_{\lambda_2,\lambda_j}, H^{Am}_{\lambda_2,\lambda_j}$ are given by

$$\begin{aligned}
H^{Vm}_{\frac{1}{2}t} &= \sqrt{\frac{Q_+}{q^2}}\,\Big(M_-\,F_1^{Vm} + \frac{q^2}{M_1}\,F_3^{Vm}\Big)\,, \\
H^{Vm}_{\frac{1}{2}1} &= \sqrt{2Q_-}\,\Big(F_1^{Vm} + \frac{M_+}{M_1}\,F_2^{Vm}\Big)\,, \\
H^{Vm}_{\frac{1}{2}0} &= \sqrt{\frac{Q_-}{q^2}}\,\Big(M_+\,F_1^{Vm} + \frac{q^2}{M_1}\,F_2^{Vm}\Big)\,, \\
H^{Am}_{\frac{1}{2}t} &= \sqrt{\frac{Q_-}{q^2}}\,\Big(M_+\,F_1^{Am} - \frac{q^2}{M_1}\,F_3^{Am}\Big)\,, \\
H^{Am}_{\frac{1}{2}1} &= \sqrt{2Q_+}\,\Big(F_1^{Am} - \frac{M_-}{M_1}\,F_2^{Am}\Big)\,, \\
H^{Am}_{\frac{1}{2}0} &= \sqrt{\frac{Q_+}{q^2}}\,\Big(M_-\,F_1^{Am} - \frac{q^2}{M_1}\,F_2^{Am}\Big)\,,
\end{aligned} \tag{C6}$$

where $M_\pm = M_1 \pm M_2$, $Q_\pm = M_\pm^2 - q^2$. The form factors F_i^{Vm}, F_i^{Am} are linear combinations of the form factors f_i^J. In case of the rare decays they involve also the Wilson coefficients. In particular, the sets of form factors F_i^{Vm}, F_i^{Am}

for the semileptonic charged current decays with the Cabibbo-allowed $b \to c$ and $c \to s$ transitions read

$$
\begin{aligned}
F_1^{V1} &= f_1^V\,, \\
F_2^{V1} &= f_2^V\,, \\
F_3^{V1} &= f_3^V\,, \\
\\
F_1^{A1} &= f_1^A\,, \\
F_2^{A1} &= f_2^A\,, \\
F_3^{A1} &= f_3^A\,.
\end{aligned}
\tag{C7}
$$

In the case of the $\Lambda_b \to \Lambda + \ell^+\ell^-$ transitions the corresponding form factors are

$$
\begin{aligned}
F_1^{V1} &= C_9^{\rm eff}\, f_1^V - \frac{2m_b}{M_1}\, C_7^{\rm eff}\, f_1^{TV}\,, \\
F_2^{V1} &= C_9^{\rm eff}\, f_2^V - \frac{2m_b M_1}{q^2}\, C_7^{\rm eff}\, f_2^{TV}\,, \\
F_3^{V1} &= C_9^{\rm eff}\, f_3^V + \frac{2m_b M_-}{q^2}\, C_7^{\rm eff}\, f_1^{TV}\,, \\
\\
F_1^{A1} &= C_9^{\rm eff}\, f_1^A + \frac{2m_b}{M_1}\, C_7^{\rm eff}\, f_1^{TA}\,, \\
F_2^{A1} &= C_9^{\rm eff}\, f_2^A + \frac{2m_b M_1}{q^2}\, C_7^{\rm eff}\, f_2^{TA}\,, \\
F_3^{A1} &= C_9^{\rm eff}\, f_3^A + \frac{2m_b M_+}{q^2}\, C_7^{\rm eff}\, f_1^{TA}\,,
\end{aligned}
\tag{C8}
$$

and

$$
\begin{aligned}
F_i^{V2} &= C_{10}\, f_i^V\,, \\
F_i^{A2} &= C_{10}\, f_i^A\,.
\end{aligned}
\tag{C9}
$$

Finally, in the case of the one-photon transitions $\Lambda_b \to \Lambda + \gamma$ one needs the helicity amplitudes $H^V_{\pm\frac12,\pm1} \equiv H^{V1}_{\pm\frac12,\pm1}$ and $H^A_{\pm\frac12,\pm1} \equiv H^{A1}_{\pm\frac12,\pm1}$ They are related to the f_2^{TV} and f_2^{TA} form factors by

$$
\begin{aligned}
H^V_{\pm\frac12,\pm1} &= \sqrt{2}\,\frac{M_+M_-}{M_1}\, F_2^V\,, \\
H^A_{\pm\frac12,\pm1} &= \mp\sqrt{2}\,\frac{M_+M_-}{M_1}\, F_2^A\,,
\end{aligned}
\tag{C10}
$$

where

$$
\begin{aligned}
F_2^V &= -C_7^{\rm eff}\,\frac{m_b}{M_1} f_2^{TV}\,, \\
F_2^A &= -C_7^{\rm eff}\,\frac{m_b}{M_1} f_2^{TA}\,.
\end{aligned}
\tag{C11}
$$

Appendix D: Wilson coefficients

In this paper we use the set of Wilson coefficients (see Table IX) fixed in Ref. [48]. The Wilson coefficient $C_9^{\rm eff}$ effectively takes into account, first, the contributions from the four-quark operators Q_i $(i = 1, ..., 6)$ and, second, the nonperturbative effects coming from the $c\bar{c}$-resonance contributions which are as usual parametrized by a Breit-Wigner ansatz [60]:

$$\begin{aligned} C_9^{\rm eff} &= C_9 + C_0 \left\{ h(\hat m_c, s) + \frac{3\pi}{\alpha^2}\,\kappa \sum_{V_i=\psi(1s),\psi(2s)} \frac{\Gamma(V_i \to l^+l^-)\, m_{V_i}}{{m_{V_i}}^2 - q^2 - i m_{V_i}\Gamma_{V_i}} \right\} \\ &- \frac{1}{2} h(1,s)\,(4C_3 + 4C_4 + 3C_5 + C_6) \\ &- \frac{1}{2} h(0,s)\,(C_3 + 3C_4) + \frac{2}{9}\,(3C_3 + C_4 + 3C_5 + C_6)\;. \end{aligned} \tag{D1}$$

where $C_0 \equiv 3C_1 + C_2 + 3C_3 + C_4 + 3C_5 + C_6$. Here

$$\begin{aligned} h(\hat m_c, s) &= -\frac{8}{9}\ln\frac{m_b}{\mu} - \frac{8}{9}\ln \hat m_c + \frac{8}{27} + \frac{4}{9}x \\ &- \frac{2}{9}(2+x)|1-x|^{1/2} \begin{cases} \left(\ln\left|\frac{\sqrt{1-x}+1}{\sqrt{1-x}-1}\right| - i\pi\right), & \text{for } x \equiv \frac{4\hat m_c^2}{s} < 1 \\ 2\arctan\frac{1}{\sqrt{x-1}}, & \text{for } x \equiv \frac{4\hat m_c^2}{s} > 1, \end{cases} \\ h(0,s) &= \frac{8}{27} - \frac{8}{9}\ln\frac{m_b}{\mu} - \frac{4}{9}\ln\, s + \frac{4}{9} i\pi\,, \end{aligned}$$

where $\hat m_c = m_c/M_{\Lambda_b}$, $s = q^2/m_{\Lambda_b}^2$ and $\kappa = 1/C_0$. In our numerical calculations we use $\mu = m_b = 4.19$ GeV, $m_c = 1.27$ GeV, $M_{J/\psi} = 3.096916$ GeV, $M_{\Psi(2S)} = 3.68609$ GeV, $\Gamma_{J/\psi} = 92.9$ keV, $\Gamma_{\Psi(2S)} = 304$ keV, $\Gamma(J/\psi \to l^+l^-) = 5.55$ keV and $\Gamma(\Psi(2S) \to l^+l^-) = 2.35$ keV.

Appendix E: Identity $f_2^{TV}(0) = f_2^{TA}(0)$

Here we demonstrate that $f_2^{TV}(0) = f_2^{TA}(0)$ in the case of a P interpolating current for the Λ-type baryons. The same statement is also true for S- and A-currents. After integration over the loop momenta k_1 and k_2 the general structure of the matrix elements involving the Dirac matrix $\Gamma^\mu = i\sigma^{\mu q}$ or $i\sigma^{\mu q}\gamma^5$ is written as

$$M^\mu(p_1,p_2) = F(p_1^2,p_2^2,q^2)\,\bar u_2(p_2)(1 + \alpha_1\, \not p_1 + \alpha_2\, \not p_2)\,\Gamma^\mu\,(1 + \beta_1\, \not p_1 + \beta_2\, \not p_2)\,u_1(p_1)\,, \tag{E1}$$

where $F(p_1^2,p_2^2,q^2)$ depends on the invariants p_1^2, p_2^2 and q^2. The α_i and β_i are coefficients whose explicit values are not needed for the proof. Using the package FORM one can show that the $f_2^{TV}(q^2)$ and $f_2^{TA}(q^2)$ form factors are given by:

$$\begin{aligned} f_2^{TV}(q^2) &= f_2^{TA}(q^2) + 2\alpha_1\beta_2 q^2\, F(p_1^2,p_2^2,q^2) \\ &= F(p_1^2,p_2^2,q^2)\left[1 + M_1(\beta_1+\beta_2) + M_2(\alpha_1+\alpha_2) + M_1M_2(\alpha_1+\alpha_2)(\beta_1+\beta_2) + \alpha_1\beta_2 q^2\right]. \end{aligned} \tag{E2}$$

Therefore, the form factors $f_2^{TV}(q^2)$ and $f_2^{TA}(q^2)$ differ only by a term linear in q^2 and therefore one has $f_2^{TV}(0) = f_2^{TA}(0)$.

---

[1] T. Aaltonen *et al.* [CDF Collaboration], Phys. Rev. Lett. **107**, 201802 (2011) [arXiv:1107.3753 [hep-ex]].
[2] H. -Y. Cheng, C. -Y. Cheung, G. -L. Lin, Y. C. Lin, T. -M. Yan and H. -L. Yu, Phys. Rev. D **51**, 1199 (1995) [hep-ph/9407303].
[3] T. Mannel, S. Recksiegel, J. Phys. G **24**, 979 (1998) [hep-ph/9701399].
[4] P. Colangelo, F. De Fazio, R. Ferrandes and T. N. Pham, Phys. Rev. D **77**, 055019 (2008) [arXiv:0709.2817 [hep-ph]].
[5] R. Mohanta, A. K. Giri, M. P. Khanna, M. Ishida and S. Ishida, Prog. Theor. Phys. **102**, 645 (1999) [hep-ph/9908291].
[6] H. -Y. Cheng and B. Tseng, Phys. Rev. D **53**, 1457 (1996); D **55**, 1697(E) (1997) [hep-ph/9502391].
[7] L. Mott and W. Roberts, Int. J. Mod. Phys. A **27**, 1250016 (2012) [arXiv:1108.6129 [nucl-th]].
[8] X. -G. He, T. Li, X. -Q. Li and Y. -M. Wang, Phys. Rev. D **74**, 034026 (2006) [hep-ph/0606025].
[9] C. S. Huang and H. G. Yan, Phys. Rev. D **59**, 114022 (1999); D **61**, 039901(E) (2000)] [arXiv:hep-ph/9811303].
[10] C. -H. Chen, C. Q. Geng, Phys. Rev. **D63** , 114024 (2001) [hep-ph/0101171].

[11] C. -H. Chen, C. Q. Geng, Phys. Lett. **B516** , 327 (2001) [hep-ph/0101201].
[12] C. -H. Chen, C. Q. Geng, Phys. Rev. **D64** , 074001 (2001) [hep-ph/0106193].
[13] F. Zolfagharpour and V. Bashiry, Nucl. Phys. B **796**, 294 (2008) [arXiv:0707.4337 [hep-ph]].
[14] F. Hussain, J. G. Körner, M. Krämer, G. Thompson, Z. Phys. **C51** , 321 (1991).
[15] F. Hussain, D. -S. Liu, M. Krämer, J. G. Körner, S. Tawfiq, Nucl. Phys. **B370** , 259 (1992).
[16] T. Mannel, W. Roberts, Z. Ryzak, Nucl. Phys. **B355** , 38 (1991).
[17] W. Detmold, C. -J. D. Lin, S. Meinel and M. Wingate, Phys. Rev. D **87**, 074502 (2013) [arXiv:1212.4827 [hep-lat]].
[18] L. -F. Gan, Y. -L. Liu, W. -B. Chen and M. -Q. Huang, Communications in Theoretical Physics **58**, 872 (2012) [arXiv:1212.4671 [hep-ph]].
[19] J. G. Körner, P. Kroll, Phys. Lett. **B293** , 201 (1992).
[20] J. G. Körner, P. Kroll, Z. Phys. **C57** , 383 (1993).
[21] P. Ball and V. M. Braun, Phys. Rev. D **55**, 5561 (1997) [hep-ph/9701238].
[22] Y. -M. Wang, Y. Li and C. -D. Lu, Eur. Phys. J. C **59**, 861 (2009) [arXiv:0804.0648 [hep-ph]].
[23] M. J. Aslam, Y. -M. Wang and C. -D. Lu, Phys. Rev. D **78**, 114032 (2008) [arXiv:0808.2113 [hep-ph]].
[24] Y. -M. Wang, M. J. Aslam and C. -D. Lu, Eur. Phys. J. C **59**, 847 (2009) [arXiv:0810.0609 [hep-ph]].
[25] T. M. Aliev, K. Azizi, M. Savci, Phys. Rev. **D81** , 056006 (2010). [arXiv:1001.0227 [hep-ph]].
[26] T. Mannel and Y. -M. Wang, JHEP **1112**, 067 (2011) [arXiv:1111.1849 [hep-ph]].
[27] W. Wang, Phys. Lett. B **708**, 119 (2012) [arXiv:1112.0237 [hep-ph]].
[28] T. Feldmann and M. W. Y. Yip, Phys. Rev. D **85**, 014035 (2012) [arXiv:1111.1844 [hep-ph]].
[29] T. M. Aliev and M. Savci, JHEP **0605**, 001 (2006). [hep-ph/0507324].
[30] K. Azizi and N. Katirci, JHEP **1101**, 087 (2011) [arXiv:1011.5647 [hep-ph]].
[31] K. Azizi and N. Katirci, Eur. Phys. J. A **48**, 73 (2012) [arXiv:1112.5242 [hep-ph]].
[32] T. M. Aliev and M. Savci, Nucl. Phys. B **863**, 398 (2012) [arXiv:1202.0398 [hep-ph]].
[33] M. A. Ivanov, M. P. Locher and V. E. Lyubovitskij, Few Body Syst. **21**, 131 (1996).
[34] M. A. Ivanov, V. E. Lyubovitskij, J. G. Körner and P. Kroll, Phys. Rev. D **56**, 348 (1997) [arXiv:hep-ph/9612463].
[35] M. A. Ivanov, J. G. Körner and V. E. Lyubovitskij, Phys. Lett. B **448**, 143 (1999) [arXiv:hep-ph/9811370]; M. A. Ivanov, J. G. Körner, V. E. Lyubovitskij, M. A. Pisarev and A. G. Rusetsky, Phys. Rev. D **61**, 114010 (2000) [arXiv:hep-ph/9911425].
[36] M. A. Ivanov, J. G. Körner, V. E. Lyubovitskij and A. G. Rusetsky, Phys. Rev. D **60**, 094002 (1999) [arXiv:hep-ph/9904421].
[37] M. A. Ivanov, J. G. Körner, V. E. Lyubovitskij, M. A. Pisarev and A. G. Rusetsky, Phys. Rev. D **61**, 114010 (2000) [arXiv:hep-ph/9911425].
[38] M. A. Ivanov, J. G. Körner, V. E. Lyubovitskij and A. G. Rusetsky, Phys. Lett. B **476**, 58 (2000) [arXiv:hep-ph/9910342].
[39] A. Faessler, T. Gutsche, M. A. Ivanov, J. G. Körner and V. E. Lyubovitskij, Phys. Lett. B **518**, 55 (2001) [hep-ph/0107205].
[40] A. Faessler, T. .Gutsche, M. A. Ivanov, J. G. Körner, V. E. Lyubovitskij, D. Nicmorus and K. Pumsa-ard, Phys. Rev. D **73**, 094013 (2006) [hep-ph/0602193].
[41] A. Faessler, T. Gutsche, B. R. Holstein, M. A. Ivanov, J. G. Körner and V. E. Lyubovitskij, Phys. Rev. D **78**, 094005 (2008) [arXiv:0809.4159 [hep-ph]].
[42] A. Faessler, T. Gutsche, M. A. Ivanov, J. G. Körner and V. E. Lyubovitskij, Phys. Rev. D **80**, 034025 (2009) [arXiv:0907.0563 [hep-ph]].
[43] T. Branz, A. Faessler, T. Gutsche, M. A. Ivanov, J. G. Körner, V. E. Lyubovitskij and B. Oexl, Phys. Rev. D **81**, 114036 (2010) [arXiv:1005.1850 [hep-ph]].
[44] T. Branz, A. Faessler, T. Gutsche, M. A. Ivanov, J. G. Körner and V. E. Lyubovitskij, Phys. Rev. D **81**, 034010 (2010) [arXiv:0912.3710 [hep-ph]].
[45] T. Gutsche, M. A. Ivanov, J. G. Körner, V. E. Lyubovitskij and P. Santorelli, Phys. Rev. D **86**, 074013 (2012) [arXiv:1207.7052 [hep-ph]].
[46] M. A. Ivanov, J. G. Körner, S. G. Kovalenko, P. Santorelli and G. G. Saidullaeva, Phys. Rev. D **85**, 034004 (2012) [arXiv:1112.3536 [hep-ph]]; S. Dubnicka, A. Z. Dubnickova, M. A. Ivanov, J. G. Körner, P. Santorelli and G. G. Saidullaeva, Phys. Rev. D **84**, 014006 (2011) [arXiv:1104.3974 [hep-ph]]; S. Dubnicka, A. Z. Dubnickova, M. A. Ivanov, J. G. Körner and G. G. Saidullaeva, AIP Conf. Proc. **1343**, 385 (2011) [arXiv:1011.4417 [hep-ph]]; S. Dubnicka, A. Z. Dubnickova, M. A. Ivanov and J. G. Körner, Phys. Rev. D **81**, 114007 (2010) [arXiv:1004.1291 [hep-ph]].
[47] A. Kadeer, J. G. Körner, U. Moosbrugger, Eur. Phys. J. **C59** , 27 (2009) [hep-ph/0511019].
[48] A. Faessler, T. Gutsche, M. A. Ivanov, J. G. Körner, V. E. Lyubovitskij, Eur. Phys. J. direct **C4** , 18 (2002) [hep-ph/0205287].
[49] P. Bialas, J. G. Körner, M. Krämer, K. Zalewski, Z. Phys. **C57** , 115 (1993).
[50] J. G. Körner and G. A. Schuler, Phys. Lett. B **231** (1989) 306; J.G. Körner and G.A. Schuler, Z. Phys. **C46**, 93 (1990).
[51] F. Krüger and J. Matias, Phys. Rev. D **71**, 094009 (2005) [hep-ph/0502060].
[52] J. Beringer *et al.* [Particle Data Group Collaboration], Phys. Rev. D **86**, 010001 (2012).
[53] J. G. Körner, M. Kramer and D. Pirjol, Prog. Part. Nucl. Phys. **33**, 787 (1994) [hep-ph/9406359].
[54] S. Weinberg, Phys. Rev. **130**, 776 (1963).
[55] A. Salam, Nuovo Cim. **25**, 224 (1962).
[56] K. Hayashi, M. Hirayama, T. Muta, N. Seto and T. Shirafuji, Fortsch. Phys. **15**, 625 (1967).
[57] G. V. Efimov and M. A. Ivanov, *The Quark Confinement Model of Hadrons*, (IOP Publishing, Bristol & Philadelphia, 1993).
[58] J. A. M. Vermaseren, Nucl. Phys. Proc. Suppl. **183**, 19 (2008) [arXiv:0806.4080 [hep-ph]]; arXiv:math-ph/0010025.

[59] G. Buchalla, A. J. Buras and M. E. Lautenbacher, Rev. Mod. Phys. **68**, 1125 (1996) [hep-ph/9512380].
[60] A. Ali, T. Mannel and T. Morozumi, Phys. Lett. B **273**, 505 (1991).
[61] G. Hiller and A. Kagan, Phys. Rev. D **65**, 074038 (2002) [hep-ph/0108074].
[62] J. R. Batley *et al.* [NA48/1 Collaboration], arXiv:1212.3131 [hep-ex].

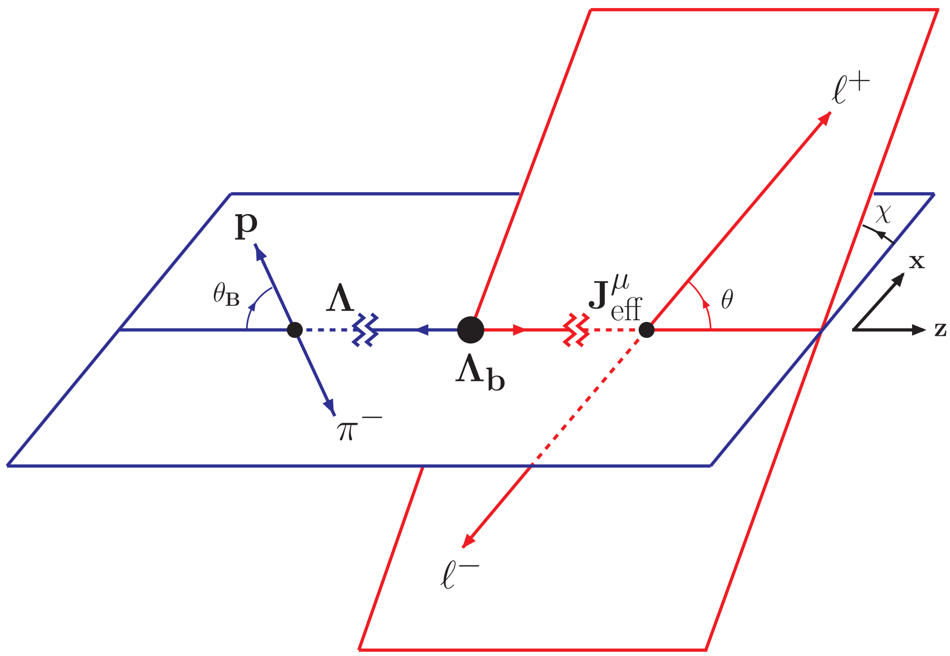

FIG. 1: Definition of angles θ, θ_B and χ in the cascade decay $\Lambda_b \to \Lambda(\to p\pi^-) + J_{\rm eff}(\to \ell^+\ell^-)$.

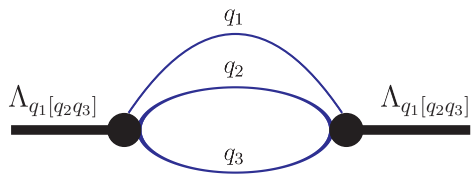

FIG. 2: $\Lambda_{q_1[q_2q_3]}$ baryon mass operator.

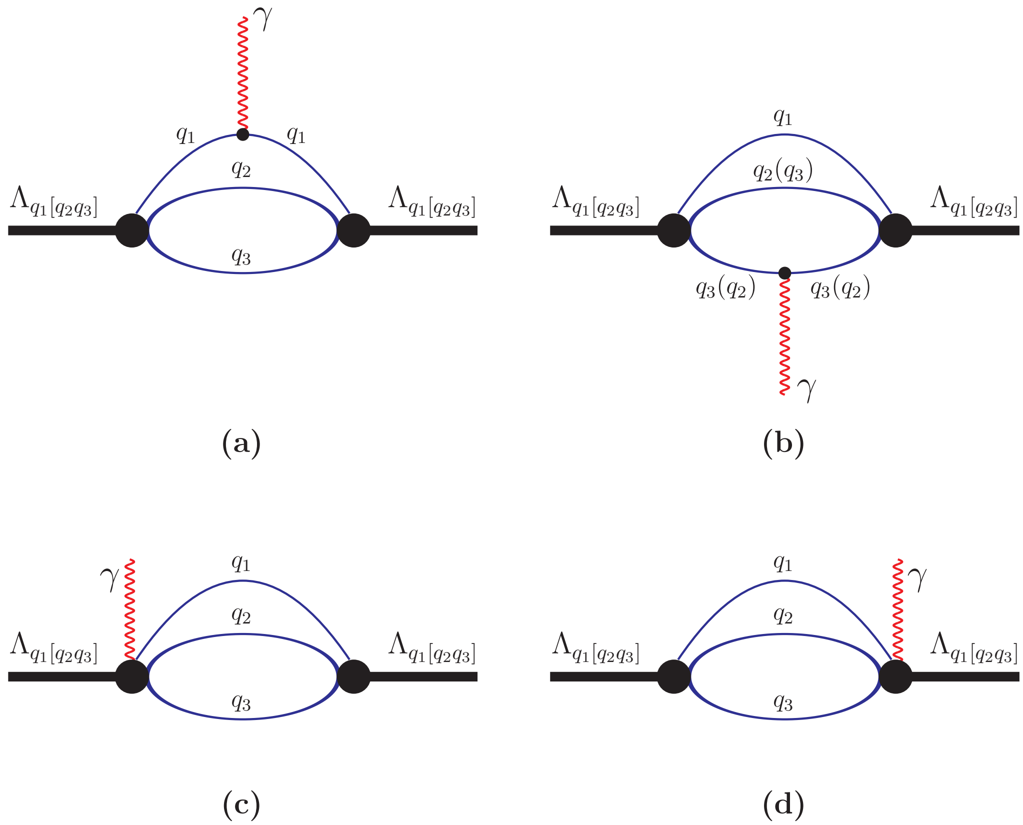

FIG. 3: Electromagnetic vertex function of the $\Lambda_{q_1[q_2q_3]}$ baryon: (a) triangle diagram with the (off-shell) photon attached to the quark q_1; (b) triangle diagram with the (off-shell) photon attached to quarks q_2 or q_3; (c) bubble diagram with the (off-shell) photon attached to the vertex of the ingoing baryon; (d) bubble diagram with the (off-shell) photon attached to the vertex of the outgoing baryon.

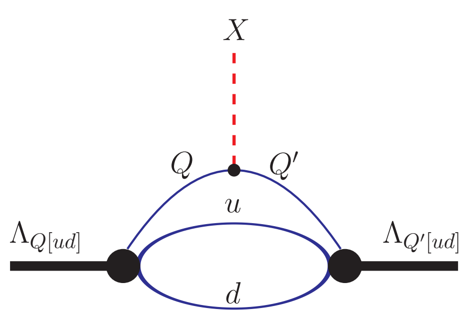

FIG. 4: Diagrams contributing to the flavor-changing transition $\Lambda_{Q[ud]} \to \Lambda_{Q'[ud]} + X$, where $X = \ell^- \bar{\nu}_\ell, \ell^+\ell^-$ or γ.

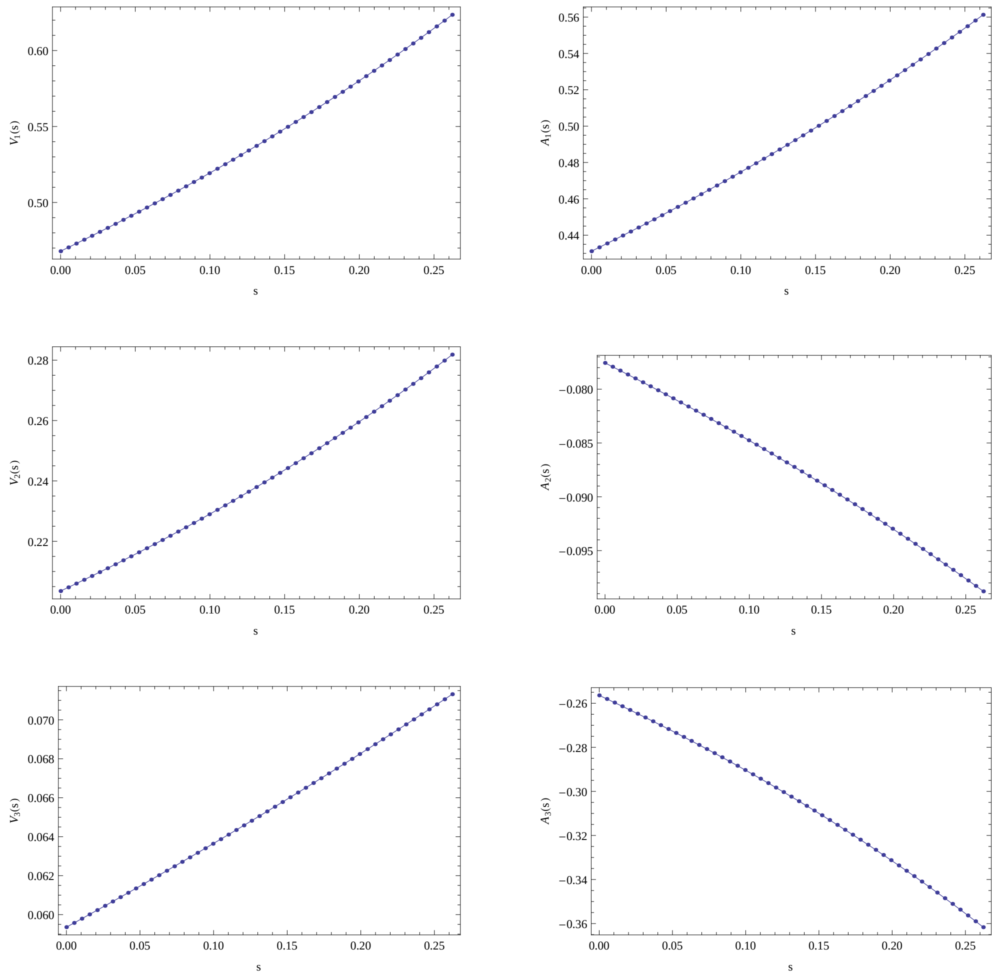

FIG. 5: Form factors defining the transition $\Lambda_c \to \Lambda$: approximated results (solid line), exact result(dotted line).

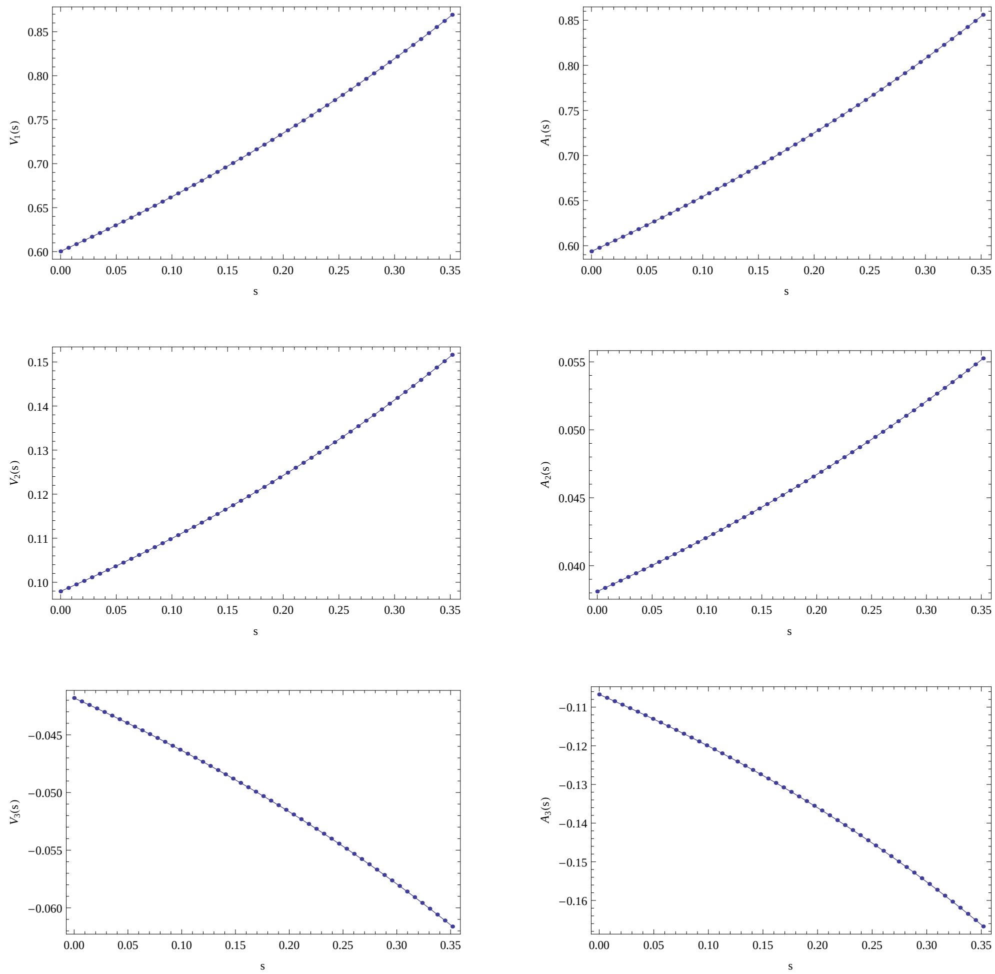

FIG. 6: Form factors defining the transition $\Lambda_b \to \Lambda_c$: approximated results (solid line), exact result (dotted line).

TABLE I: Parameters for the approximated form factors $f(s) = f(0)/(1 - as + bs^2)$, $s = q^2/m^2_{\Lambda_b}$ in the $\Lambda_c \to \Lambda$ transition.

	f_1^V	f_2^V	f_3^V	f_1^A	f_2^A	f_3^A
$f(0)$	0.468	0.204	0.059	0.431	-0.078	-0.256
a	1.017	1.148	0.698	0.939	0.870	1.208
b	0.249	0.337	0.221	0.211	0.195	0.377

TABLE II: Parameters for the approximated form factors $f(s) = f(0)/(1 - as + bs^2)$, $s = q^2/m^2_{\Lambda_b}$ in the $\Lambda_b \to \Lambda_c$ transition.

	f_1^V	f_2^V	f_3^V	f_1^A	f_2^A	f_3^A
$f(0)$	0.600	0.098	0.042	0.594	0.038	-0.107
a	0.961	1.127	1.008	0.951	0.971	1.148
b	0.233	0.344	0.267	0.228	0.254	0.357

TABLE III: Parameters for the approximated form factors $f(s) = f(0)/(1 - as + bs^2)$, $s = q^2/m^2_{\Lambda_b}$ in the $\Lambda_b \to \Lambda$ transition.

	f_1^V	f_2^V	f_3^V	f_1^A	f_2^A	f_3^A	f_1^{TV}	f_2^{TV}	f_1^{TA}	f_2^{TA}
$f(0)$	0.107	0.043	0.003	0.104	0.003	-0.052	-0.043	-0.105	0.003	-0.105
a	2.271	2.411	2.815	2.232	2.955	2.437	2.411	0.072	2.955	2.233
b	1.367	1.531	2.041	1.328	3.620	1.559	1.531	0.001	3.620	1.328

TABLE IV: Branching ratios of semileptonic decays of heavy baryons (in %).

Mode	Our results	Data [52]
$\Lambda_c \to \Lambda e^+ \nu_e$	2.0	2.1 ± 0.6
$\Lambda_c \to \Lambda \mu^+ \nu_\mu$	2.0	2.0 ± 0.7
$\Lambda_b \to \Lambda_c e^- \bar{\nu}_e$	6.6	$6.5^{+3.2}_{-2.5}$
$\Lambda_b \to \Lambda_c \mu^- \bar{\nu}_\mu$	6.6	
$\Lambda_b \to \Lambda_c \tau^- \bar{\nu}_\tau$	1.8	

TABLE V: Asymmetry parameter α in the semileptonic decays of heavy baryons.

Mode	Our results	Data [52]
$\Lambda_c \to \Lambda e^+ \nu_e$	0.828	0.86 ± 0.04
$\Lambda_c \to \Lambda \mu^+ \nu_\mu$	0.825	
$\Lambda_b \to \Lambda_c e^- \bar{\nu}_e$	0.831	
$\Lambda_b \to \Lambda_c \mu^- \bar{\nu}_\mu$	0.831	
$\Lambda_b \to \Lambda_c \tau^- \bar{\nu}_\tau$	0.731	

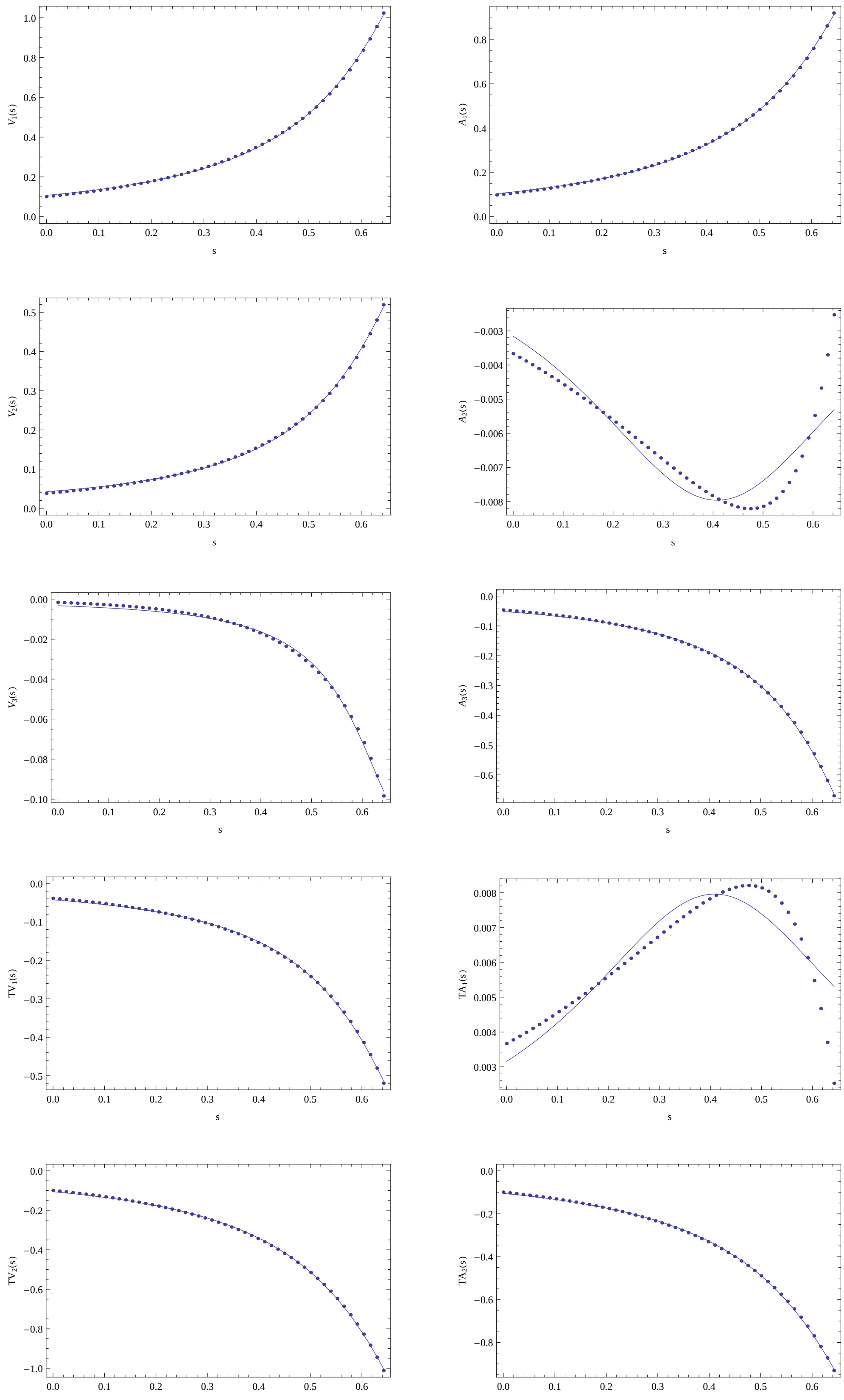

FIG. 7: Form factors defining the transition $\Lambda_b \to \Lambda$: approximated results (solid line), exact result (dotted line).

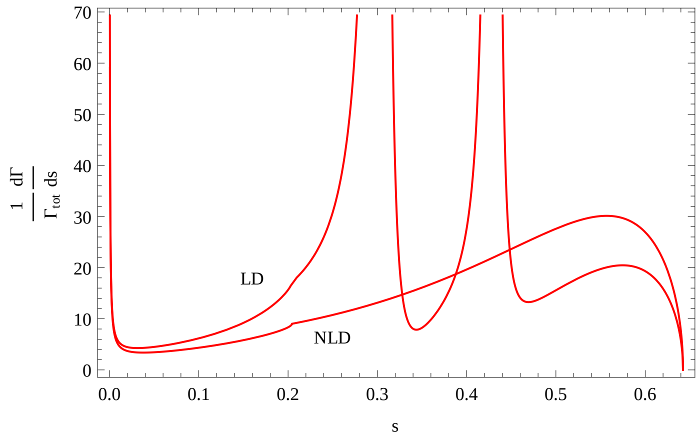

FIG. 8: Differential rate $\frac{1}{\Gamma_{\rm tot}} \frac{d\Gamma(\Lambda_b \to \Lambda\, e^+ e^-)}{ds}$ in units of 10^{-7} GeV^{-2}.

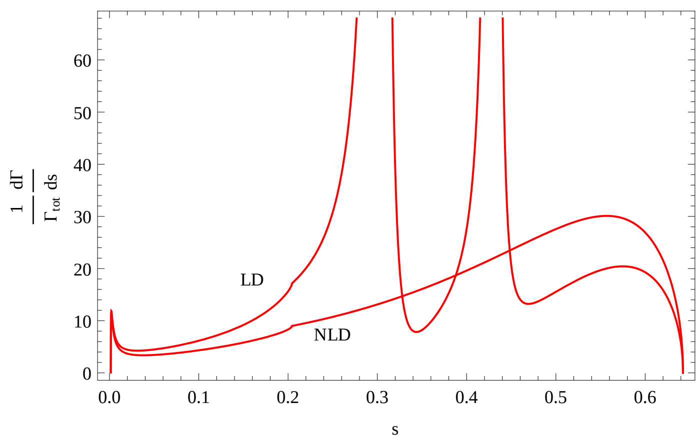

FIG. 9: Differential rate $\frac{1}{\Gamma_{\rm tot}} \frac{d\Gamma(\Lambda_b \to \Lambda\, \mu^+ \mu^-)}{ds}$ in units of 10^{-7} GeV^{-2}.

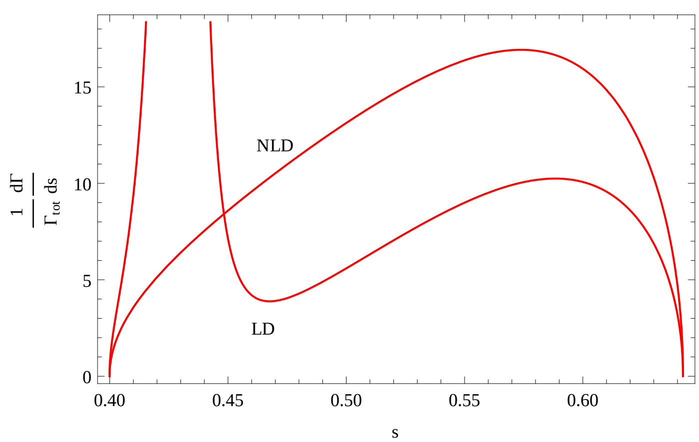

FIG. 10: Differential rate $\frac{1}{\Gamma_{\rm tot}} \frac{d\Gamma(\Lambda_b \to \Lambda\, \tau^+ \tau^-)}{ds}$ in units of 10^{-7} GeV^{-2}.

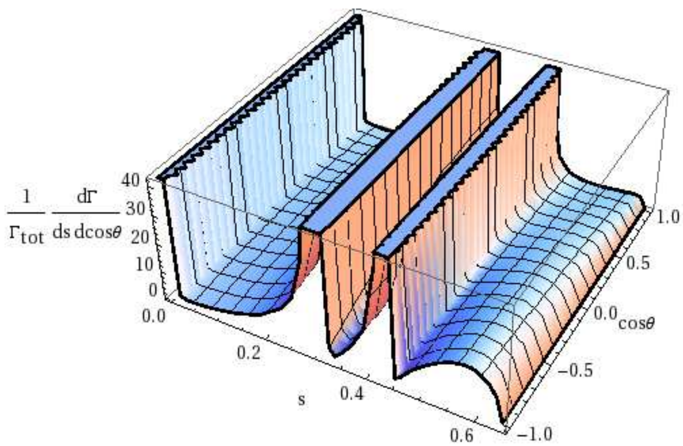

FIG. 11: Lepton-side angular decay distribution $\frac{1}{\Gamma_{\rm tot}} \frac{d\Gamma(\Lambda_b \to \Lambda\, e^+ e^-)}{ds\, d\cos\theta}$ in units of 10^{-7} GeV^{-2}.

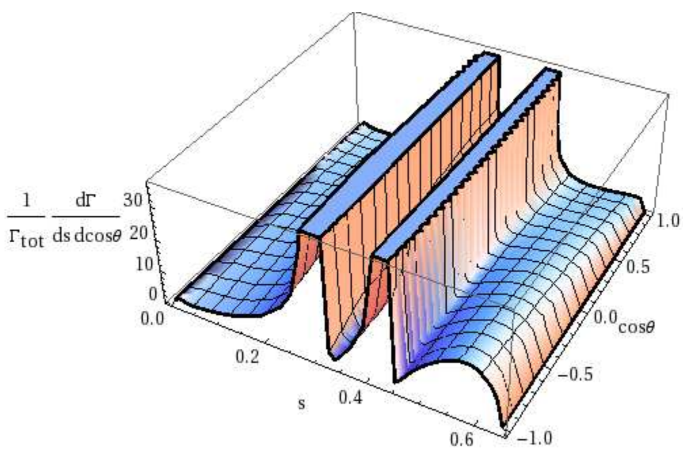

FIG. 12: Lepton-side angular decay distribution $\frac{1}{\Gamma_{\rm tot}} \frac{d\Gamma(\Lambda_b \to \Lambda\, \mu^+ \mu^-)}{ds\, d\cos\theta}$ in units of 10^{-7} GeV^{-2}.

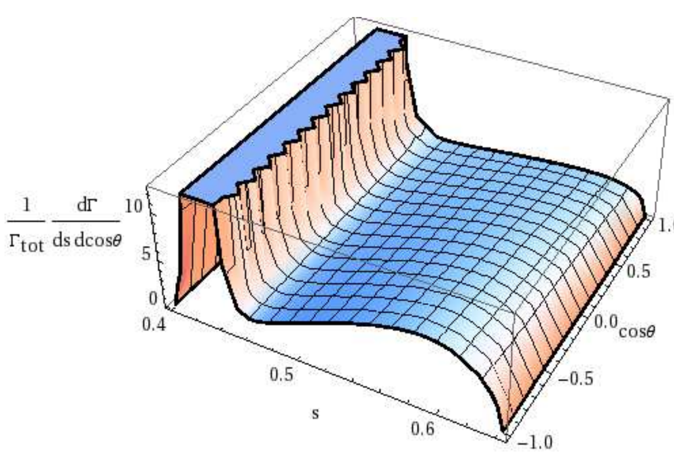

FIG. 13: Lepton-side angular decay distribution $\frac{1}{\Gamma_{\rm tot}} \frac{d\Gamma(\Lambda_b \to \Lambda\, \tau^+ \tau^-)}{ds\, d\cos\theta}$ in units of 10^{-7} GeV^{-2}.

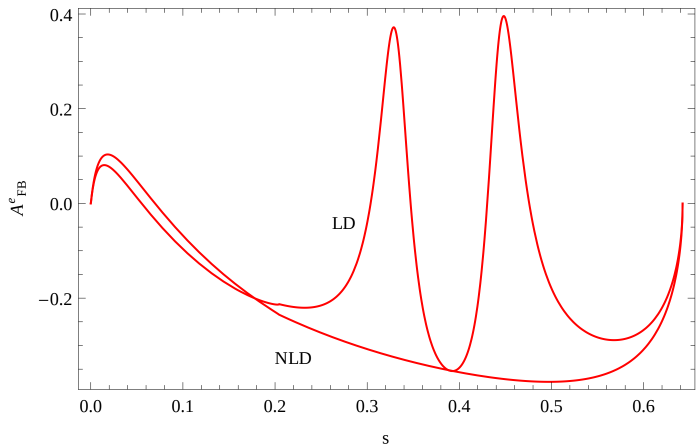

FIG. 14: Lepton–side forward–backward asymmetry A^l_{FB} in the decay $\Lambda_b \to \Lambda\, e^+e^-$.

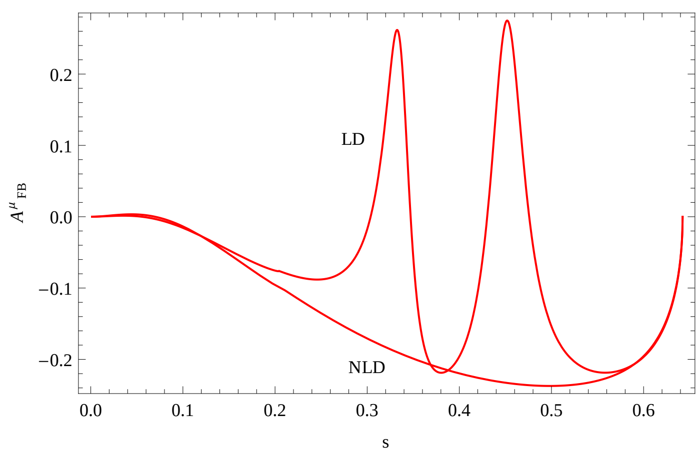

FIG. 15: Lepton–side forward–backward asymmetry A^l_{FB} in the decay $\Lambda_b \to \Lambda\, \mu^+\mu^-$.

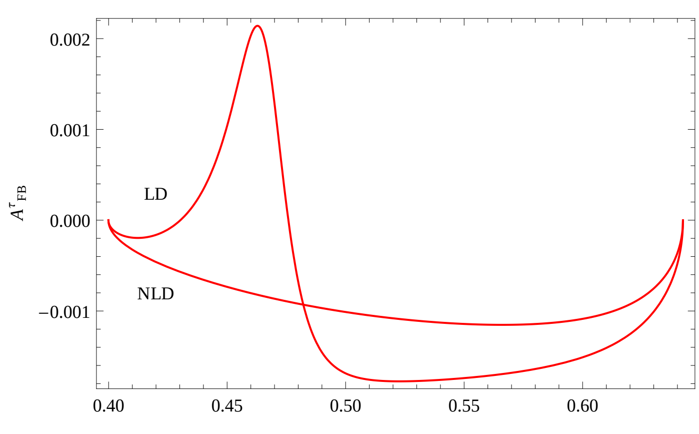

FIG. 16: Lepton–side forward–backward asymmetry A^l_{FB} in the decay $\Lambda_b \to \Lambda\, \tau^+\tau^-$.

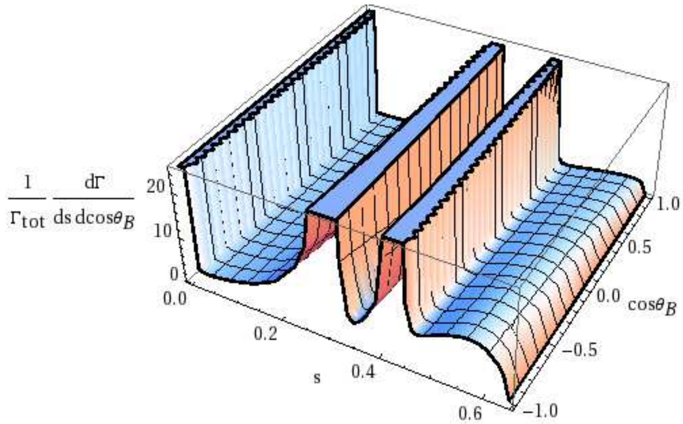

FIG. 17: Hadron-side angular decay distribution $\frac{1}{\Gamma_{\rm tot}} \frac{d\Gamma(\Lambda_b \to \Lambda\, e^+ e^-)}{ds d\cos\theta_B}$ in units of 10^{-7} GeV^{-2}.

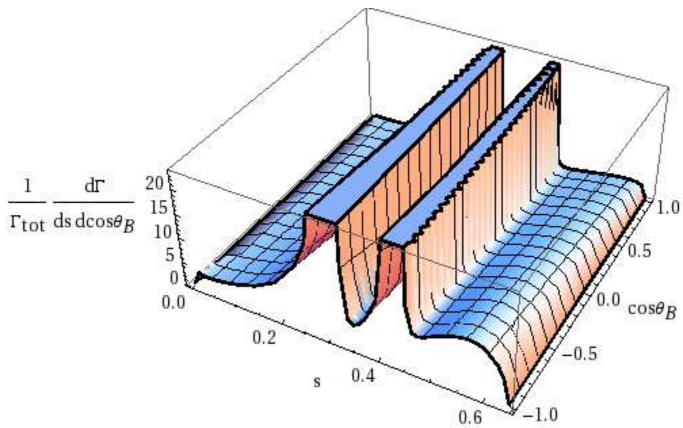

FIG. 18: Hadron-side angular decay distribution $\frac{1}{\Gamma_{\rm tot}} \frac{d\Gamma(\Lambda_b \to \Lambda\, \mu^+ \mu^-)}{ds d\cos\theta_B}$ in units of 10^{-7} GeV^{-2}.

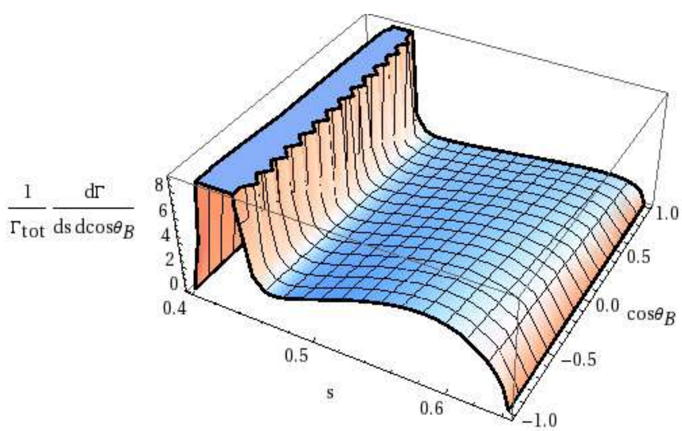

FIG. 19: Hadron-side angular decay distribution $\frac{1}{\Gamma_{\rm tot}} \frac{d\Gamma(\Lambda_b \to \Lambda\, \tau^+ \tau^-)}{ds d\cos\theta_B}$ in units of 10^{-7} GeV^{-2}.

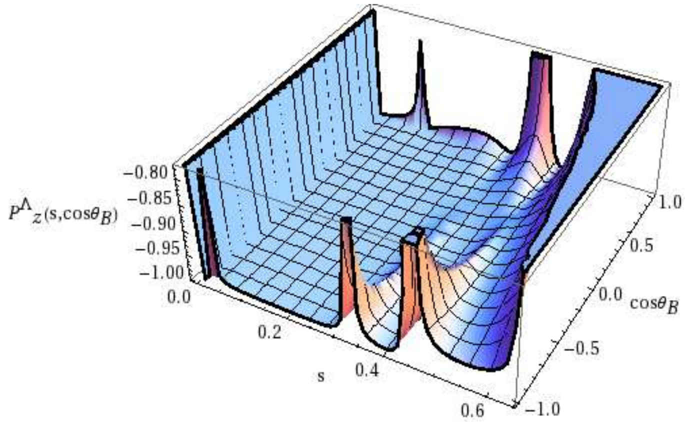

FIG. 20: Polarization $P_z^\Lambda(s, \cos\theta_B)$ for the decay $\Lambda_b \to \Lambda\, e^+e^-$.

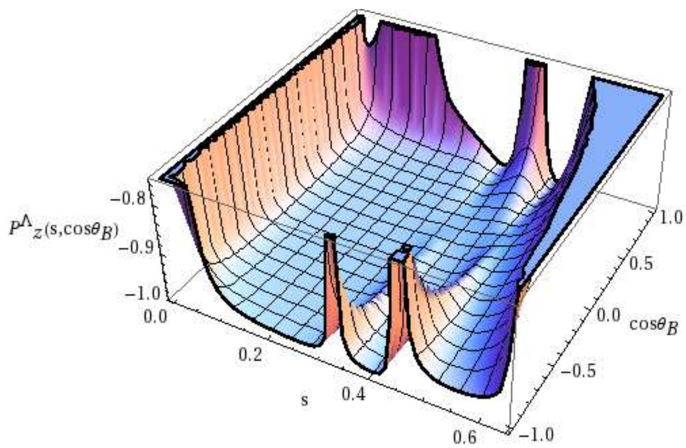

FIG. 21: Polarization $P_z^\Lambda(s, \cos\theta_B)$ in the decay $\Lambda_b \to \Lambda\, \mu^+\mu^-$.

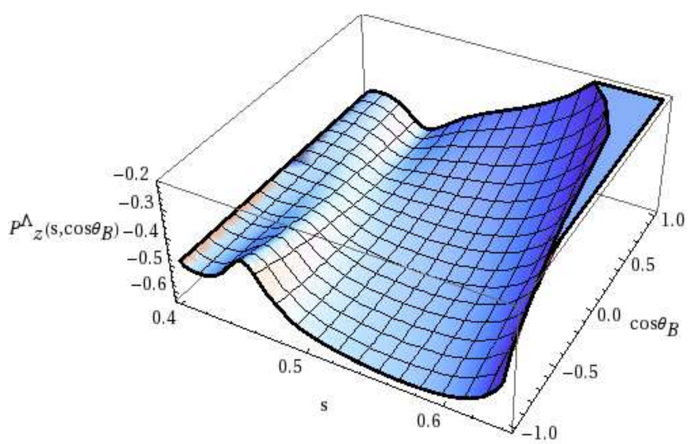

FIG. 22: Polarization $P_z^\Lambda(s, \cos\theta_B)$ in the decay $\Lambda_b \to \Lambda\, \tau^+\tau^-$.

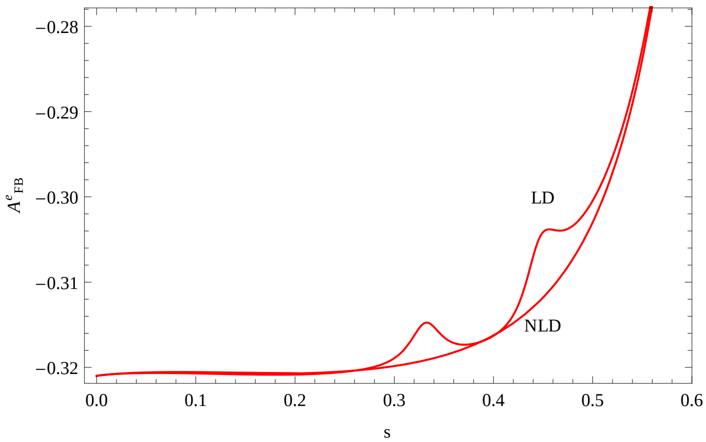

FIG. 23: Hadron–side forward–backward asymmetry A^h_{FB} in the decay $\Lambda_b \to \Lambda\, e^+ e^-$.

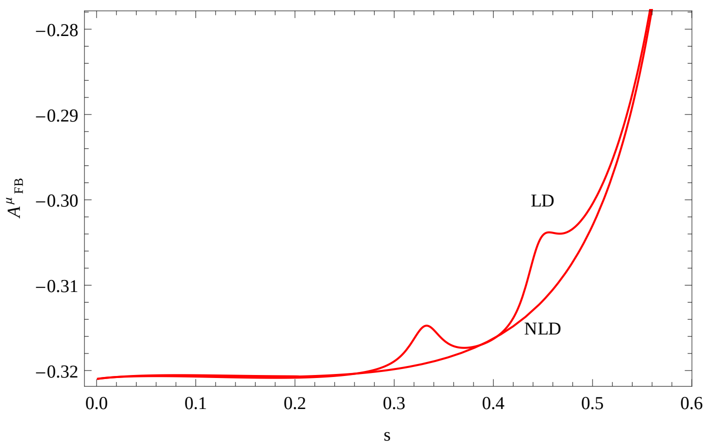

FIG. 24: Hadron–side forward–backward asymmetry A^h_{FB} in the decay $\Lambda_b \to \Lambda\, \mu^+ \mu^-$.

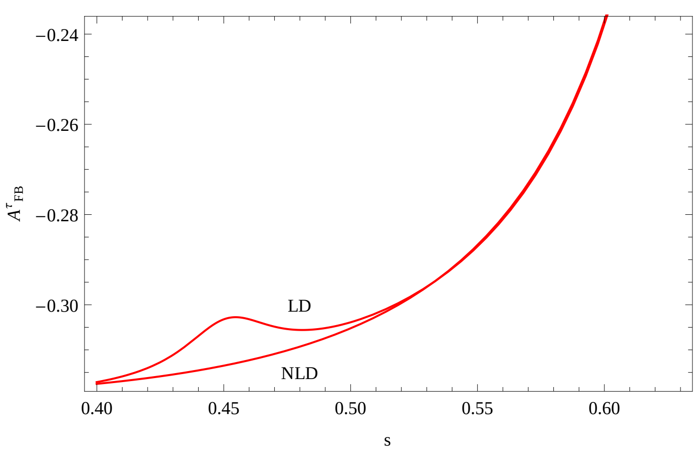

FIG. 25: Hadron–side forward–backward asymmetry A^h_{FB} in the decay $\Lambda_b \to \Lambda\, \tau^+ \tau^-$.

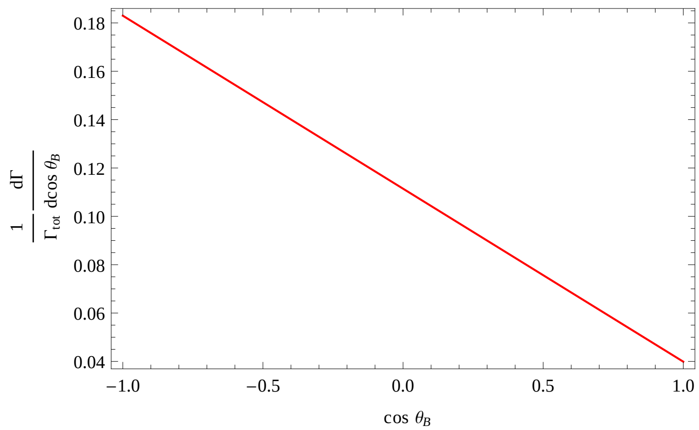

FIG. 26: Angular decay distribution for the decay $\Lambda_b \to \Lambda(\to p\pi^-)\gamma$ in units of 10^{-5}.

TABLE VI: Branching ratios of semileptonic decays $\Lambda_b \to \Lambda\ell^+\ell^-$ with (without) long–distance contributions (in units of 10^{-6}).

Mode	Our results	Theoretical predictions	Data
$\Lambda_b \to \Lambda e^+e^-$	1.0 (1.0)	2.79 ± 0.56 [12]; 4.6 ± 1.6 [25]; 53 (2.3) [10]	
$\Lambda_b \to \Lambda\mu^+\mu^-$	1.0 (1.0)	26.5 ± 5.5 (0.8 ± 0.2) [7]; 53 (2.1) [10]; 2.64 ± 0.56 [12]; 46 (6.1) [22]; 39 (5.9) [23]; 4.0 ± 1.2 [25]; $3.96^{+0.38}_{-0.08}$ [18]; $2.03^{+0.26}_{-0.09}$ [18]	1.73 ± 0.42 ± 0.55 [1]
$\Lambda_b \to \Lambda\tau^+\tau^-$	0.2 (0.3)	0.63 ± 0.13 (0.30 ± 0.08) [7]; 0.23 ± 0.05 [12]; 4.3 (2.4) [22]; 4.0 (2.1) [23]; 0.8 ± 0.3 [25]; 11 (0.18) [10]	

TABLE VII: Branching ratio of the radiative decay $\Lambda_b \to \Lambda\gamma$ (in units of 10^{-5}).

Our result	Theoretical predictions	Data [52]
0.4	2.75 ± 1.75 [3]; 3.7 ± 0.5 [9]; 3.1 ± 0.6 [10]; 0.68 ± 0.05 [24]; $1.99^{+0.34}_{-0.31}$ [18]; $0.61^{+0.14}_{-0.13}$ [18]; 1.55±0.35 [2]; 0.6 [2]; 0.23 [5]; 5.55±1.25 [8]	< 130

TABLE VIII: Asymmetries $\bar{A}^l_{FB}$ and $\bar{A}^h_{FB}$ with (without) long–distance contributions.

Mode	$\bar{A}^l_{FB}$	$\bar{A}^h_{FB}$
$\Lambda_b \to \Lambda e^+e^-$	3.2×10^{-10} (1.2×10^{-8})	-0.321 (-0.321)
$\Lambda_b \to \Lambda\mu^+\mu^-$	1.7×10^{-4} (8.0×10^{-4})	-0.300 (-0.294)
$\Lambda_b \to \Lambda\tau^+\tau^-$	5.9×10^{-4} (9.6×10^{-4})	-0.265 (-0.259)

TABLE IX: Values of Wilson coefficients.

C_1	-0.248	C_4	-0.026	$C_7^{\rm eff}$	-0.313
C_2	1.107	C_5	0.007	C_9	4.344
C_3	0.011	C_6	-0.031	C_{10}	-4.669